Universiteit Utrecht

Master Thesis

The local climate on the East Antarctic Plateau in relation to large scale flow patterns

Author:
L.G. Bohn

Supervisors:
Dr Carleen Tijm-Reijmer
Dr Aarnout van Delden

Institute for Marine and Atmospheric research Utrecht
Department of Physics
Utrecht University

2021CE July 16

Abstract

Although the density of observation sites is low on the East Antarctic Plateau, there are several locations at which meteorological observations are conducted. These observations provide insights into the local climate, and are invaluable for evaluating climate models and satellite observations. Additionally, the ERA5 reanalysis dataset from the European Centre for Medium-range Weather Forecasts (ECMWF) may enable these records to be extended with longer time series and far more complete spatial coverage, providing further insights into local climate conditions. The main purpose of this study is to obtain a better understanding of the variability and trends in local climate on the East Antarctic Plateau, and therefore better understand how conditions on the East Antarctic Plateau react to changes in climate. The first step toward this goal is to assess the agreement between observational records and ERA5 data for the parameters of interest – air temperature, surface pressure, and wind speed – in order to determine whether the ERA5 data are suitable for extending these records. The next step is to analyze the available data by examining climatological averages, comparing conditions at different sites, and investigating variability and trends. In the final step, local variables are examined in relation to indices representing two large-scale atmospheric flow patterns that are known to impact the Antarctic climate: the Southern Annular Mode (SAM) index and the Southern Oscillation Index (SOI).

Despite the fact that comparisons between observations and ERA5 data are imperfect, there is often fairly good agreement between them, particularly for air temperature and surface pressure. While no statistically significant temporal trends are found in monthly mean (potential) temperature at any site for either observations or ERA5, some significant temporal trends are found for wind speed in both datasets at some sites, which could be connected to an upward trend in the SAM in recent decades. Both linear regression correlations and empirical orthogonal function (EOF) analysis show the effects of the SAM to be far more prominent than those of the SO in this region. Both (potential) temperature and wind speeds are found to decrease with high SAM index values – when the meridional pressure gradient is stronger between Antarctica and lower latitudes – while any impact from the SO seems absent or negligible. Whether either the SAM or SO has an effect on snow accumulation in this region is unclear.

Contents

Acknowledgments

First, I want to thank Dr Carleen Tijm-Reijmer, whose weekly guidance and encouragement made every part of this project possible. Whether by answering questions, or by asking them. Whether by inspiring ambition, or the maintaining of realistic expectations. By showing me which direction to go, or by helping me trust that I already knew the way forward. Thanks also to Dr Aarnout van Delden, for providing valuable feedback at some critical points during the project.

I am also very grateful to my friends and study group here in the UU Climate Physics program: Emma, Handi, Julia, Lena, Miriam, Ruben, and Sophie. For listening to my exultations and depressions and everything between, and inviting me to listen to all the same from them. For helping me take breaks, whether for fifteen minutes or five hours; whether I felt like I needed one or not, I always did. For providing a place to be my very strange self. And for many good chats about many good books (and sometimes other topics).

Finally, thanks to all the friends, family, and mentors who have supported me, wherever they reside. For their interest in my studies, or at least for patiently listening to me explain what I am studying. And for all the many acts of encouragement and kindness that helped me get to this point, in ways large and small – far too numerous to list, but which I hope they each are aware of. Among them, special thanks go to my grandfather, John Bohn, who was able to see only the start of this project and not its conclusion, but who always believed I would be a good scientist someday.

Plain-English Summary

East Antarctica is home to the largest body of ice on Earth, which could eventually contribute more than any other to rising sea levels. Thus, it is crucial to understand how the East Antarctic ice responds to changes in climate. However, away from the coasts, about 3 km above sea level on the East Antarctic Plateau, we find one of the harshest environments on Earth, and one where there is still much to discover.

In this study, we are mainly concerned with the temperature, wind speed, and snowfall at or near the surface of the East Antarctic Plateau. Our goal is to investigate how the conditions here are influenced by two large-scale patterns of air movement in the atmosphere that span much of the southern half of the globe. These patterns are called the SAM and the SO (short for 'Southern Annular Mode' and 'Southern Oscillation'). Each of them alternates between two states, which we call the 'positive phase' and the 'negative phase'. The different phases of each should have opposite effects on the weather of the East Antarctic Plateau.

To explore how these things are connected, we use two kinds of data. One is measurements taken in the field, either by automatic weather stations designed to take measurements without any human input, or by scientists and technicians working at crewed research stations. Another is from a simulation called the ERA5 that uses field data as a guide to help it simulate the weather. For temperature and air pressure, the station data and ERA5 agreed very well. Wind at the stations was not measured at the same height that ERA5 simulates, and how high off the ground (or ice) we look makes a large difference for how fast the wind will be, so wind speeds did not agree as precisely as the temperatures and air pressures did. The two also did not agree about snow, since the uncrewed weather stations measure the total result of snow falling and being blown away, but ERA5 only simulates how much snow falls.

For both the station data and ERA5 data, we find that wind speeds seem to be changing over time in some places. Winds closer to the surface of the ice seem to be getting weaker over time at some of the stations, but wind at the height that ERA5 simulates seems to be growing stronger. Neither source of data showed evidence that temperature or amounts of snow are changing over time, but there might be changes happening that are difficult to detect.

There was little sign from either the stations or the ERA5 of the SO affecting temperature, wind speed, or snow in this region. The SO is known to affect the weather in and around Antarctica, but it might not reach the East Antarctic Plateau. There could also still be effects that we were not able to see using the techniques we used to look for them.

Data from the stations and from ERA5 all showed strong evidence that the SAM affects temperatures on the East Antarctic Plateau, with the positive phase causing unusually low temperatures and the negative phase causing unusually high temperatures. The ERA5 data also showed evidence that the positive SAM phase causes weaker winds, and that the negative SAM phase causes stronger winds in the region. The station data did not show much sign of the SAM affecting wind speeds, and neither the stations nor ERA5 data suggested that snow on the East Antarctic Plateau is being altered by the SAM. Taken together, this all suggests that the SAM does have an influence on the temperature on the East Antarctic Plateau, might affect wind differently at different heights near the surface of the ice, and we are not sure whether the SAM affects snow in the region or not. The evidence we did find for how the SAM changes the weather of the East Antarctic Plateau is exactly what we expect based on what other scientists have found before.

Glossary of abbreviations

AWI Alfred Wegener Institute

AWS Automatic Weather Station

DML Dronning Maud Land (a.k.a. Queen Maud Land)

ECMWF European Centre for Medium-range Weather Forecasts

ENSO El Niño–Southern Oscillation

EOF Empirical Orthogonal Function

EPICA European Project for Ice Coring in Antarctica

ERA5 ECMWF ReAnalysis, generation 5

IMAU Institute for Marine and Atmospheric research Utrecht

MSLP Mean Sea-Level Pressure

Plateau (capitalized) East Antarctic Plateau

READER REference Antarctic Data for Environmental Research

RMSD Root-Mean-Square-Difference

SAM Southern Annular Mode (may also refer to the SAM index)

SO Southern Oscillation

SOI Southern Oscillation Index

1 Introduction

East Antarctica holds the largest body of ice on Earth, and thus is the dominant factor in potential eventual sea-level rise. Therefore, understanding how the East Antarctic Ice Sheet responds to climate forcing is crucial. Despite this, the East Antarctic Plateau in particular is under-studied relative to the Antarctic Peninsula, West Antarctica, and the coastal regions of East Antarctica. In-situ observations are sparse due to the difficulty of traveling or maintaining permanent research stations on the Plateau (hereafter, *Plateau* or *the Plateau* will be used in this study to refer to the East Antarctic Plateau). Studies conducted with the data available have found either no significant temperature trends in East Antarctica, or sometimes weak cooling trends in some areas (Lazzara et al., 2012; Marshall et al., 2013; Smith and Polvani, 2017)[16][19][32]. Such results are found regardless of the widespread warming observed in the Antarctic Peninsula and West Antarctica (Bromwich et al., 2013, 2014; Carrasco, 2013; Schneider et al., 2012a)[4][5][6][28], and despite the fact that amplified temperature increases are expected in the polar regions (Holland and Bitz, 2003; Serreze et al., 2009)[11][31].

The atmosphere over the Plateau is thin, and has low concentrations of clouds, water vapor, and aerosols, making it highly transmissive to solar radiation (van den Broeke et al., 2006)[37]. However, because the Plateau has a high surface albedo, only $5 - 20\%$ of incoming solar radiation is absorbed by the ice sheet surface (van den Broeke et al., 2006)[37]. Warming of the surface due to incoming solar radiation is more than compensated by radiative cooing during the nights and winters, since the cold and dry atmosphere and clear skies allow a net loss of heat due to long-wave radiation emitted by the surface. Because sensible heat flux acts to decrease the temperature difference between the surface and the atmospheric boundary layer, radiative cooling of the surface also indirectly cools the boundary layer, which then becomes denser. The presence of this negatively buoyant boundary layer means that the surface slope is a major factor in the climate of the ice sheet, since the slope induces katabatic wind, which then affects surface energy flux via turbulent heat transport and impacts the snow surface itself by enhancing sublimation and snowdrift. The katabatic wind causes a divergence of air at the surface, transporting air away from the Plateau and toward the edges of the continent; this is compensated by transport of air masses toward the inland that occurs higher in the atmosphere, and which provides influx of heat and moisture to Antarctica. This poleward transport of air is partially obstructed by the circumpolar vortex: the band of tropospheric westerly winds which surround Antarctica as a result of the atmospheric pressure gradient between Antarctica and the lower latitudes.

One of the major climate variability modes in the Antarctic and southern midlatitudes is the Southern Annular Mode (SAM), which is characterized by a roughly annulus-shaped spatial pattern of opposite-sign pressure and temperature anomalies over the southern middle and high latitudes (Marshall, 2007)[18], illustrated in Figure 1 in the form of a difference plot of annual sea-level pressure for positive and negative SAM phases. The positive phase of the SAM corresponds to negative pressure anomalies in the southern high-latitudes and positive pressure anomalies over the southern midlatitudes; with the negative phase of the SAM corresponding to the reverse. During the positive SAM phase, there is a larger-than-average pressure gradient between the high- and mid-latitudes of the southern hemisphere, which results in a weakening of the katabatic flow over the continent and a stronger circumpolar vortex (Jones et al., 2019; Marshall and Bracegirdle, 2015)[14][20]. The presence of these stronger westerly winds further reduces meridional mixing of air masses, and this together with the weakened katabatic flow results in less heat and moisture being advected to the

Plateau (Jones et al., 2019; Marshall and Bracegirdle, 2015)[14][20]. As the Plateau surface and boundary layer continue to lose heat through radiative processes, the result is a stronger temperature inversion in the Plateau boundary layer, and therefore lower surface temperatures (Jones et al., 2019; Marshall and Bracegirdle, 2015)[14][20]. Inversely, the negative phase of the SAM is associated with warmer temperatures on the Plateau (Jones et al., 2019)[14]. The effects of the SAM on Antarctic temperatures are visualized in Figure 2 as the difference in mean daily surface air temperature anomalies between the positive and negative SAM phases.

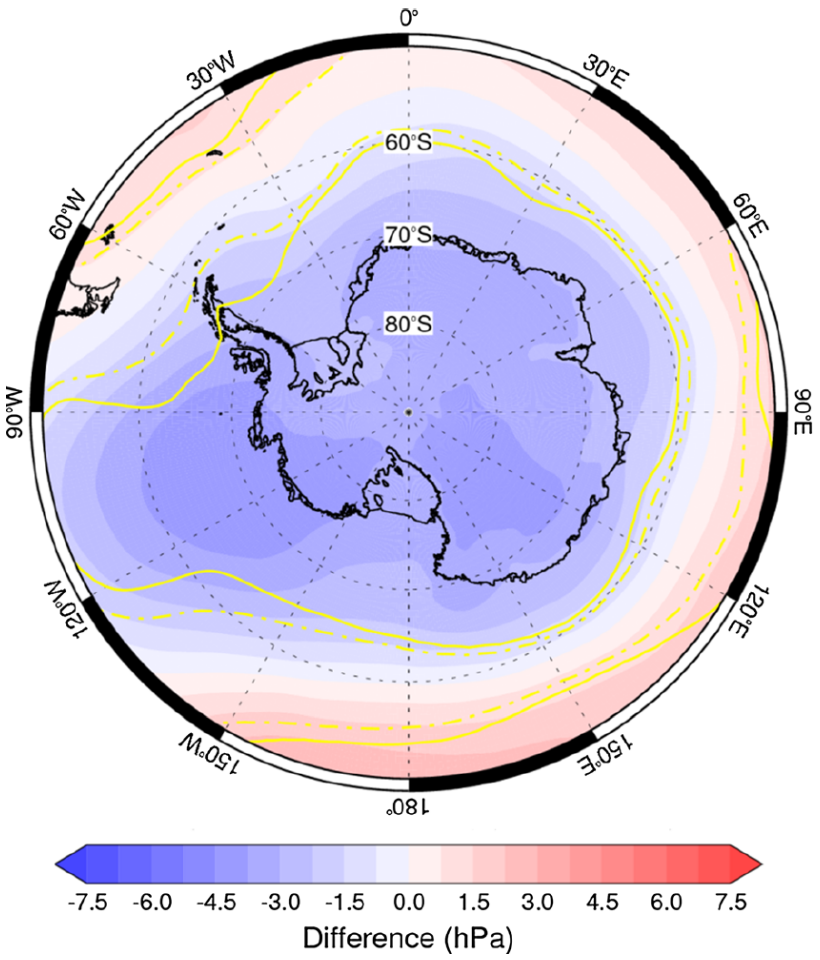

Figure 1: Difference plot of annual annual sea level pressure (SLP) between positive and negative SAM (*top/bottom* ranked 8 years from the 1979–2003CE period). The SAM data are from Marshall (2003) and the SLP data from the ERA–Interim reanalysis. *Full* and *dashed lines* represent a statistically significant difference at $p < 0.05$ and $p < 0.10$, respectively. Reprinted from Marshall and Bracegirdle (2015), Figure 9a [20].

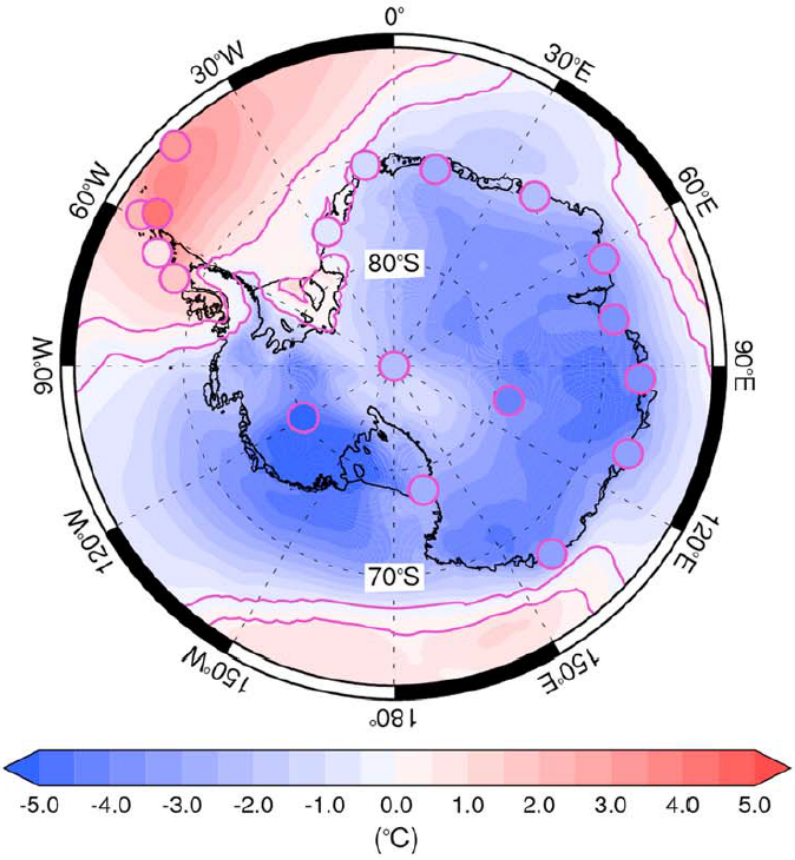

Figure 2: Differences in mean daily surface air temperature anomalies across all seasons between the positive and negative phases of the SAM. The purple contour represents regions where the difference is significant at the $p < 0.05$ level. Similarly, stations where the difference is significant at the $p < 0.05$ level are represented as purple circles. Reprinted from Marshall and Thompson (2016), Figure 3b [21].

A positive SAM phase could also be associated with competing effects on snow accumulation, depending on location. The weakened katabatic flow could result in less accumulation in locations where katabatic winds deposit drifting snow, but could also mean less removal of snow by katabatic wind-driven snow drifting. Meanwhile, the reduced advection of moisture to the atmosphere over the Plateau is expected to reduce precipitation across the region. Inversely, a negative SAM phase could result in more accumulation or more snow removal from drifting due to stronger katabatic winds, and could increase precipitation on the Plateau due to increased moisture advection to the region.

Due to a combination of stratospheric ozone depletion, increased greenhouse gas concentration, and natural variability, in recent decades the SAM has been trending toward the positive phase during austral summer and autumn (Fogt and Marshall, 2020)[9]. Because of this trend, the influence of the SAM on the Plateau climate could contribute to possible downward trends in temperatures, winds speeds, and snowfall on the Plateau. In particular, a SAM-driven lowering of temperatures could help explain why the expected background warming has been difficult to detect in this region.

The observational SAM index data used in this study and its definition are introduced in section

2.2.2, and the calculation used to derive a SAM index from ERA5 data is discussed in section 3.3.

Another important climate mode in the southern hemisphere is the Southern Oscillation (SO): the atmospheric component of the El Niño–Southern Oscillation (ENSO), with the positive SO phase corresponding to the La Niña phase and the negative SO phase to El Niño. Because both are defined based on pressure anomalies in overlapping regions, the SAM and the SO are not fully independent from each other, and it can be difficult to separate their impacts (Welhouse et al. 2016)[38]. Impacts of these modes on the Antarctic climate have been found to be amplified when the modes are in opposite phases, i.e. positive SAM phase and negative SO phase, or negative SAM and positive SO (Fogt et al., 2011)[8]. The influence of the SO in East Antarctica is strongest during austral summer (Schneider et al., 2012b)[29]. Four mechanisms connect the negative SO phase with reduced poleward advection of heat in the South Atlantic sector (Yuan et al. 2018)[39], any or all of which could also be applicable to parts of East Antarctica:

1. Trains of Rossby waves, originating in the tropical pacific, causing anomalous high pressure in the Amundsen Sea
2. Contrasting sea surface temperature anomalies in the tropical Atlantic and tropical Pacific causing zonally asymmetric meridional circulations, which weaken the Hadley cell in the South Atlantic
3. The storm tracks in the South Atlantic shifting poleward
4. Weakening of the Ferrel cell in the South Atlantic

This reduction in advection links the negative SO phase with lower temperatures and reduced moisture in some parts of the Antarctic (Kwok and Comiso, 2002)[15]. Inversely, a positive SO phase is associated with increased poleward advection of heat and moisture, contributing to higher temperatures and more snowfall.

The observational SO index data used in this study and its definition are introduced in section 2.2.3, and the method used to derive an SO index from ERA5 data is discussed in section 3.3.

The goal of this study is to use a combination of Antarctic weather station data and ERA5 reanalysis products, in order to explore the variability and trends in the climate of the Plateau and how the Plateau climate is driven by the SAM and the SO, and thereby to gain insight into how conditions on the Plateau respond to changes in the global climate system. The main meteorological variables under examination are (potential) temperature, wind speed, and snow accumulation, with surface pressure being of secondary concern due to being needed to calculate potential temperature.

Because the ERA5 datasets provide longer time series than most of the available observational records from the Plateau, the first stage is to investigate the agreement between observations and ERA5 data, whenever comparisons are possible (section 4). If sufficient agreement is found, then ERA5 products can be regarded as extended counterparts to the observational records, allowing later stages in the investigation to be applied to longer time periods. For the latter two stages, the results for observational data are discussed in section 5, and the results for ERA5 products are discussed in section 6. The next stage is to analyze the climate, variability, and trends of (potential) temperature, wind speed, and snow accumulation on the Plateau. This includes an examination of monthly climatological averages and using using pairs of station sites to illustrate how conditions differ throughout the region (sections 5.1 and 6.1) and an investigation of variability and trends for the time series of each parameter (5.2 and 6.2). The final stage is to examine how local meteorological variables at the station sites are related to the SAM and the SO, using indices

representing these oscillations (introduced in sections 2.2.2 and 2.2.3). This begins with checking for correlations between each meteorological variable and each index (5.3.1 and 6.3.1), and continues by using empirical orthogonal function (EOF) analysis to explore the connections between each meteorological variable and the SAM and SO indices as a three-parameter system (5.3.2 and 6.3.2).

2 Data

2.1 East Antarctic Plateau station data

Due to the sparsity of in-situ observations on the Plateau, the meteorological records available for this study are limited. IMAU Automatic Weather Stations provide records at four Plateau sites (section 2.1.1), while the READER archive offers data from two permanent research stations on the Plateau (2.1.2). Records at additional sites are available from other sources, but due to constraints of time and scope, such records are not utilized for this study.

Section 2.2 introduces the other data used in this study, apart from observational Plateau meteorology records. These include from the ECMWF's ERA5 reanalysis (section 2.2.1), and the observation-based SAM and SO indices and their definitions (sections 2.2.2 and 2.2.3).

2.1.1 IMAU Automatic Weather Stations

The Ice and Climate group of Utrecht University's Institute for Marine and Atmospheric research Utrecht (IMAU) operates a number of Automatic Weather Stations (AWS) on Antarctica. Including those no longer operational, IMAU has operated 19 Antarctic AWS in total since 1996CE. For this study of the Plateau climate, data from AWS 8, 9, 12, and 13 are used, all of which are of IMAU's Type II AWS design (Figure 3), with AWS 9, 12, and 13 using a special version of the Type II AWS design that is adapted for extreme low temperatures (below $-50°C$). A map of the locations and summary of the locations, elevations, and operational periods of all stations used in this study are presented at the end of this section in Figure 4 and Table 1.

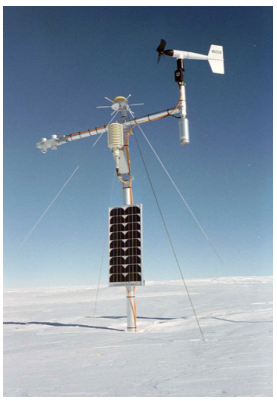

(a)

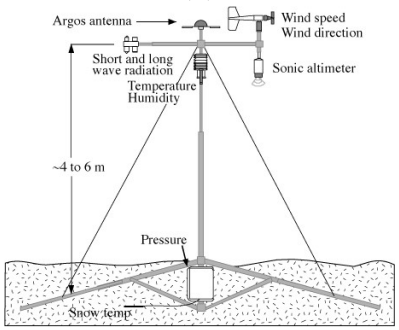

(b)

Figure 3: **(a):** AWS9, one of IMAU's Type II Automatic Weather Stations, 2002CE. **(b):** Diagram of IMAU Type II AWS design. (IMAU Ice and Climate group, n.d)[12][13]

AWS8 was located at Camp Victoria, where in January 1998 the SWEDARP expedition drilled a medium-deep ice core and erected AWS8, and it was visited several times by Alfred Wegener Institute (AWI) personnel. AWS9 is located at site DML05 of the AWI pre-site surveys for the European Project for Ice Coring in Antarctica (EPICA). In 1997CE, a medium-deep ice core was drilled at site DML05, and the EPICA DML drilling was later performed several kilometers eastward, at Kohnen station. AWI personnel erected AWS9 and visit it almost every year. (IMAU Ice and Climate group, n.d)[12]

AWS 12 and 13 were erected during International Polar Year 2007-2008CE by the Norwegian-US Scientific Traverse of East Antarctica team as they journeyed across the ice from Troll Station to Amundsen-Scott South Pole Station. AWS12 was placed 115 km North of the inactive Plateau Station, and AWS13 was placed at the Antarctic pole of inaccessibility (IMAU Ice and Climate group, n.d)[12]. Part of the Trans-Antarctic Scientific

Traverse Expeditions – Ice Divide of East Antarctica and the International Partners in Ice Coring Sciences, the Norwegian-US traverse had four stated goals: investigating the 1yr-scale to 1kyr-scale climate variability in DML; understanding spatial and temporal variability of snow accumulation in DML and its impact on sea level; investigating the impacts of atmospheric and oceanic variability on the chemical composition of firn and ice in DML; revisiting locations first explored by traverse teams in the 1960s CE, in an attempt to detect possible changes and establish benchmark data sets (Norwegian-U.S. Scientific Traverse of East Antarctica, n.d.) [27].

Data from the AWS were acquired through direct correspondence with C.H. Tijm-Reijmer of IMAU's Ice and Climate group. Each AWS provides hourly observations of wind direction (degrees clockwise from geographic north), wind speed (m s^{-1}), incoming and outgoing short-wave and long-wave radiation (W m^{-2}), air temperature (°C), relative humidity (%), air pressure (hPa), and sonic ranger height (m) as an indicator of snow accumulation.

A few factors reduce the reliability of AWS measurements compared to relatively permanent crewed research stations. The extreme conditions in Antarctica can impair the functionality of the sensors, which do not always operate perfectly in such low temperatures. The formation of rime on the sensors is not an uncommon cause of malfunction, and since an AWS may be unattended for years, the removal of rime is often a matter of chance, dictated by wind, sublimation, and gravity. As a result, measurements may be less accurate than under ideal conditions, and gaps in the data can occur.

Another such factor is data transmission and retrieval. Since the on-board data loggers from AWS 12 and 13 have not yet been retrieved, the data available from these stations were transmitted through the Argos satellite system. This makes them less precise, since they are limited in how many digits they can send, and also makes them prone to missing samples. At each transmission opportunity, these stations transmitted the sample available at that moment. Their hourly value for a given hour is therefore based on linear interpolation/extrapolation using the two closest samples within ±2 hours of that time.

Due to data transmission errors, surface pressure data from both AWS 12 and 13 are missing. Wind speed data from AWS13 are also effectively absent, as the sensor ceased to function after approximately two months. AWS8 data for temperature and wind speed are of poor quality throughout the year 1999CE, resulting in large gaps after quality control was applied (section 3.2); data for other variables and locations exhibit smaller periods that also result in gaps following quality control.

This study focuses on the time series for air temperature, wind speed, and sonic ranger height, with air pressure also being used in order to calculate potential temperature (section 3.1). For AWS9 prior to 2008CE and for AWS8, temperature and wind speed were sampled every 5 minutes, and the values reported were averages of all samples taken over the last 120 minutes, while sonic ranger height and air pressure were sampled and reported every 120 minutes. For AWS9 starting in 2008CE and for AWS 12 and 13, temperature and wind speed were sampled every 6 minutes, and the values reported were averages of all samples taken over the last 60 minutes, while sonic ranger height and air pressure were sampled and reported every 60 minutes.

2.1.2 READER archive

Monthly mean near-surface air temperature, wind speed, and air pressure records are provided by the online REference Antarctic Data for Environmental Research (READER) archive (Turner

et al. 2004)[33]. READER provides quality-controlled monthly mean time series from multiple Antarctic stations, based on four daily measurements (00, 06, 12, 18) for each variable; for surface values, READER requires that the set of samples for a given month must be at least 90% complete in order to calculate the monthly mean for that month. The records used in this study are from Amundsen-Scott South Pole Station (henceforth *Amundsen-Scott Station* or *Amundsen-Scott*) and Vostok Station, since these are the two stations on the Plateau for which READER provides records. A map of the locations and summary of the locations, elevations, and operational periods of all stations used in this study is given at the end of this section in Figure 4 and Table 1.

Amundsen-Scott Station provides the longest continuous set of meteorological data available from the Plateau. The original South Pole facilities were constructed to support research during the International Geophysical Year of 1957-1958CE, and the station has been expanded and redeveloped several times since. Approximately 50 personnel winter at Amundsen-Scott each year, and it can accommodate up to 150 personnel in summer. Research conducted there is varied, and includes astronomy, astrophysics, biology, biomedicine, climate, geophysics, and glaciology. It is named for the leaders of the first two expeditions to reach the South Pole – Roald Amundsen in 1911CE and Robert F. Scott in 1912CE – and is administered by the United States Antarctic Program division of the US National Science Foundation. (National Science Foundation, n.d.)[26]

Vostok Station provides another long meteorological record from the Plateau, with only three interruptions (1962 Jan. to 1963 Jan., 1994 Feb. to Nov., and austral winter of 2003, CE). It began operations in December of 1957CE, located above the subglacial Lake Vostok, 450 km from the highest region of the Plateau and 1260 km from the nearest coast; it lies at the Pole of Cold, where on 21 July 1983CE the lowest reliably recorded natural temperature on Earth, $-89.2°$C, was observed (Turner et al., 2009)[34]. The station's activities include meteorological and atmospheric observations and deep ice core drilling, and it is administered by the Russian Arctic and Antarctic Research Institute. (Arctic and Antarctic Research Institute, n.d.)[1]

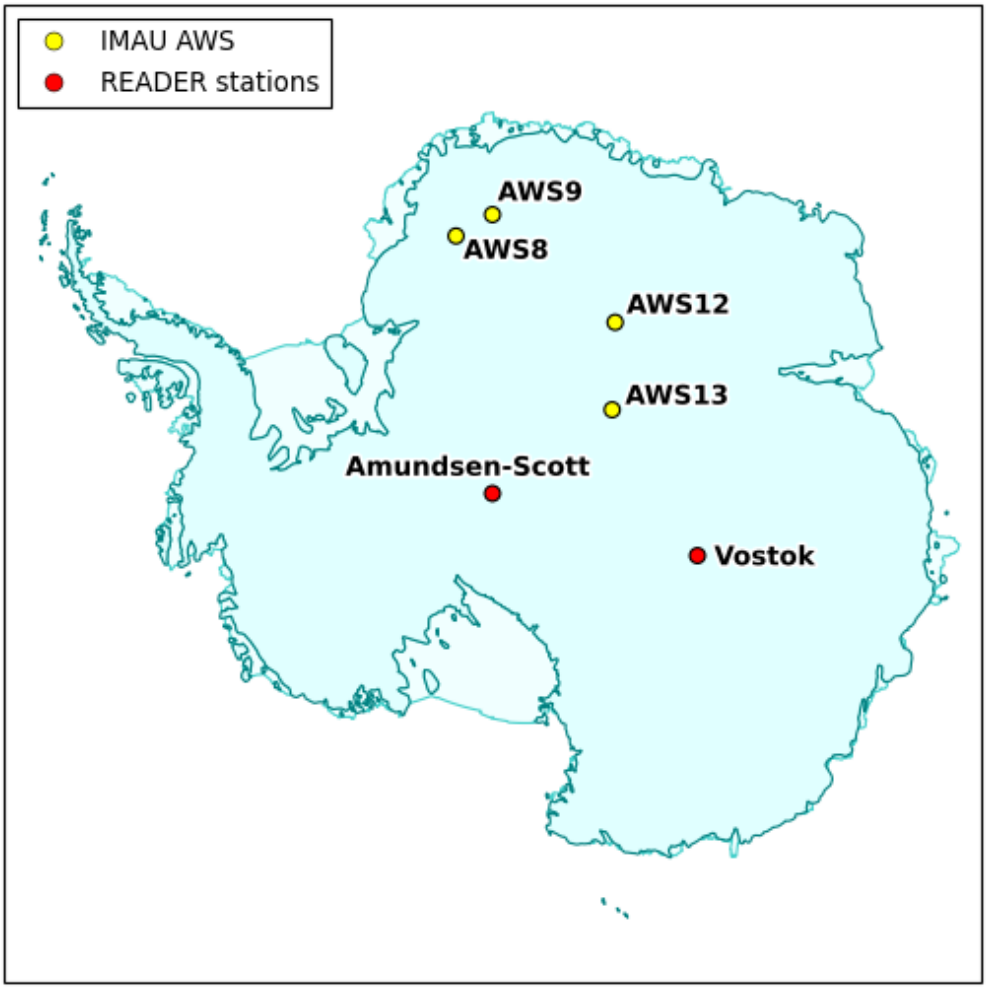

Figure 4: Map of Antarctic stations used in this study.

Table 1: Locations, approximate elevations above sea level, and operational periods of the East Antarctic Plateau stations used in this study (Arctic and Antarctic Research Institute, n.d.; IMAU Ice and Climate group, n.d.; Turner et al., 2004)[1][12][33].
*: Station remains operational as of time of writing of this report; dates given represent the period of data used in this study.

Station	Location	Elevation (m a.s.l.)	Observation period (CE)
AWS8	76°00'S, 08°03'W	~2400	1998 Jan. to 2003 Jan.
AWS9	75°00'S, 00°00'E	~2900	1997 Dec. to 2020 Sep.*
AWS12	78°39'S, 35°38'E	~3620	2007 Dec. to 2016 Mar.
AWS13	82°07'S, 55°02'E	~3730	2008 Jan. to 2016 Mar.
Amundsen-Scott	90°00'S, 00°00'E	~2835	1957 Jan. to 2020 Dec.*
Vostok	78°27'S, 106°52'E	~3488	1958 Jan. to 2020 Dec.*

2.2 Additional data

2.2.1 ERA5 reanalysis

Reanalysis assimilates decades-long observational records from across the globe into its model. The goal is to obtain a global dataset with spatial coverage far superior to what observations alone can provide, while also constraining the model with observational data to improve its accuracy. However, this dependence on observational records can be a difficulty of reanalysis, since changes in data coverage can have a large impact on the quality of the results. It can be challenging for reanalysis to reliably reproduce the conditions in regions for which observations are sparse, particularly before the start of the modern satellite era in 1979CE (Bromwich and Fogt, 2004)[3].

The ERA5 is the latest (fifth-generation) ECMWF global meteorological reanalysis, currently covering the years from 1979CE to present. Released in 2019CE, ERA5 is a higher-resolution replacement for the ERA-Interim reanalysis dataset, which covered the same time period. In addition to its higher resolution, when ERA5 is complete it will cover years 1950CE to present.

Time series for monthly mean 10m wind speeds (zonal and meridional components), 2m air temperature, surface pressure, and snowfall were obtained from the *ERA5-Land monthly averaged data from 1981 to present* dataset, provided by the ECMWF through the Copernicus Climate Data Store [24]. This dataset has a native horizontal resolution of 9 km, and is regridded to a regular $0.1° \times 0.1°$ regular lat-lon grid. Data for this study were requested for the location of each Antarctic station, accurate to within two significant digits (Table 2).

Table 2: ERA5 coordinates used for each station site.

Station	Coordinates
AWS8	76.00°S, 8.05°W
AWS9	75.00°S, 0.00°E
AWS12	78.65°S, 35.63°E
AWS13	82.12°S, 55.03°E
Amundsen-Scott	89.90°S, 0.00°E
Vostok	78.45°S, 106.87°E

Additionally, sea-level pressure time series were acquired from the *ERA5 monthly averaged data on single levels from 1979 to present* dataset from the Copernicus Climate Data Store [10]. This dataset has been regridded to a $0.25° \times 0.25°$ regular lat-lon grid for atmospheric values; this study uses sea-level pressure time series at 40°S and 65°S at all zonal grid points in order to derive a SAM index time series, and sea-level pressure time series at 12.44°S, 130.84°E (Darwin) and 17.67°S, 149.42°W (Tahiti) are used to derive an SOI time series (section 3.3).

2.2.2 Southern Annular Mode index

In order to quantify the state of the SAM, it is necessary to define a SAM index. This study uses monthly SAM index values provided by the British Antarctic Survey for 1957 Jan. to 2020 Dec. CE (Marshall, n.d.)[22], calculated using the same method as in Marshall's 2003 paper on the SAM [17]. This calculation is based on mean sea level pressure (MSLP) observations at six meteorological stations at approximately 40°S: Marion Island, Île Nouvelle Amsterdam, Hobart, Ōtautahi/Christchurch, Puerto Montt, and Gough Island – and six stations at approximately 65°S: the Antarctic stations Novolazarevskaya, Mawson, Mirny, Casey, Dumont d'Urville, and Faraday. The locations of these twelve stations are shown in Figure 5.

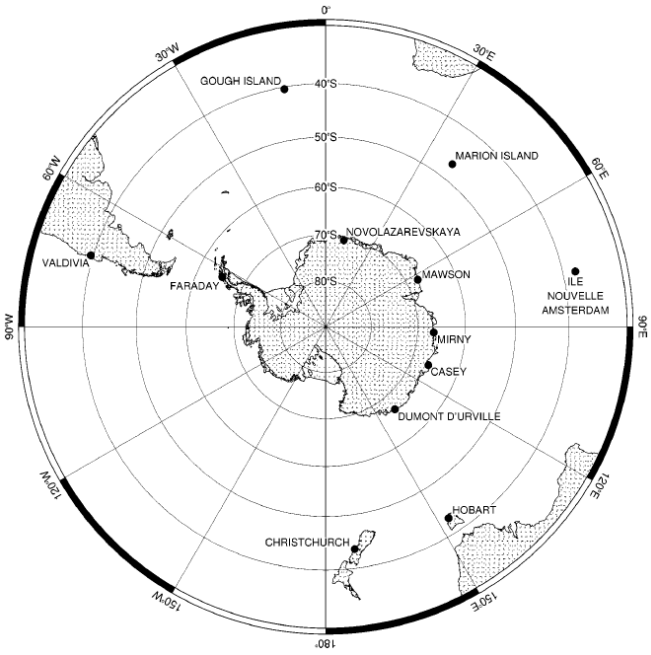

Figure 5: Stations used to calculate the observational SAM index. Reprinted from Marshall (2003), Figure 1 [17].

The monthly means of these observations are used to approximate the zonal mean monthly mean MSLP at 40°S and 65°S. The SAM index is then defined as

$$SAM = P^*_{40°S} - P^*_{65°S},$$

where the P^* are the standardized zonal mean monthly mean MSLP time series, defined as

$$P^*(t) = \frac{P(t) - \mu_P}{\sigma_P}$$

where μ_P and σ_P are the mean and standard deviation of the zonal mean monthly mean time series P, respectively.

The resulting monthly SAM index time series is shown in Figure 6; it will be compared with a SAM index derived from ERA5 data in section 4.4, and section 5.3 will investigate its relationship to observations of (potential) temperature, wind speed, and snow accumulation.

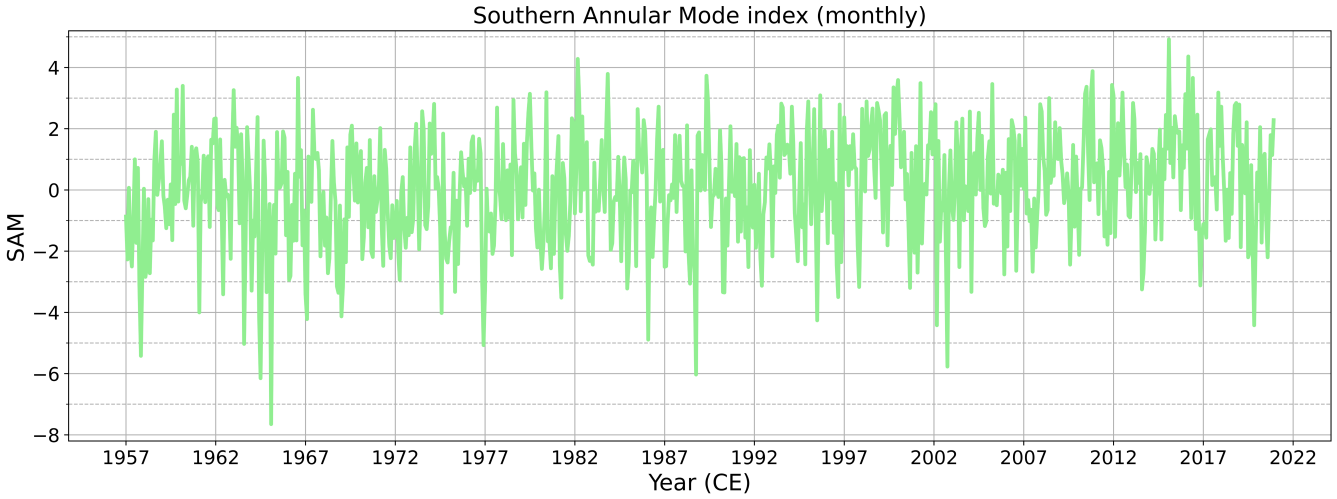

Figure 6: SAM index time series derived from observations of MSLP, provided by the British Antactic Survey (Marshall, n.d.)[22].

2.2.3 Southern Oscillation index

As with the SAM, a Southern Oscillation Index (SOI) must be defined in order to quantify the state of the SO. This study uses monthly SOI values acquired from the website of the US National Oceanic and Atmospheric Administration's National Centers for Environmental Information for 1951 Jan. to 2020 Dec. CE [25]. These index values are derived from observed sea level pressures at Darwin, Australia and at Tahiti (subscripts D and T, respectively). Each sea level pressure time series is standardized with respect to the 1981-2010CE mean values, and the index is then defined as the standardized difference of the standardized values. That is,

$$SOI = \frac{P_T^* - P_D^*}{MSD},$$

where for $A \in \{D, T\}$, P_A^* is defined as

$$P_A^* = \frac{P_{A,obs} - \bar{P}_{A,[1981,2010]}}{SD_A},$$

where

$$SD_A = \left(\frac{\sum \left(P_{A,obs} - \bar{P}_{A,[1981,2010]} \right)^2}{N} \right)^{\frac{1}{2}}$$

is the standard deviation with respect to the 1981-2010CE mean, with number of months N, and where the monthly standard deviation MSD is given by (National Centers for Environmental Information, n.d.)[25]

$$MSD = \left(\frac{\sum \left(P_T^* - P_D^* \right)^2}{N} \right)^{\frac{1}{2}}.$$

The resulting monthly SOI time series is shown in Figure 7; it will be compared with a SOI derived from ERA5 data in section 4.4, and section 5.3 will investigate its relationship to observations of (potential) temperature, wind speed, and snow accumulation.

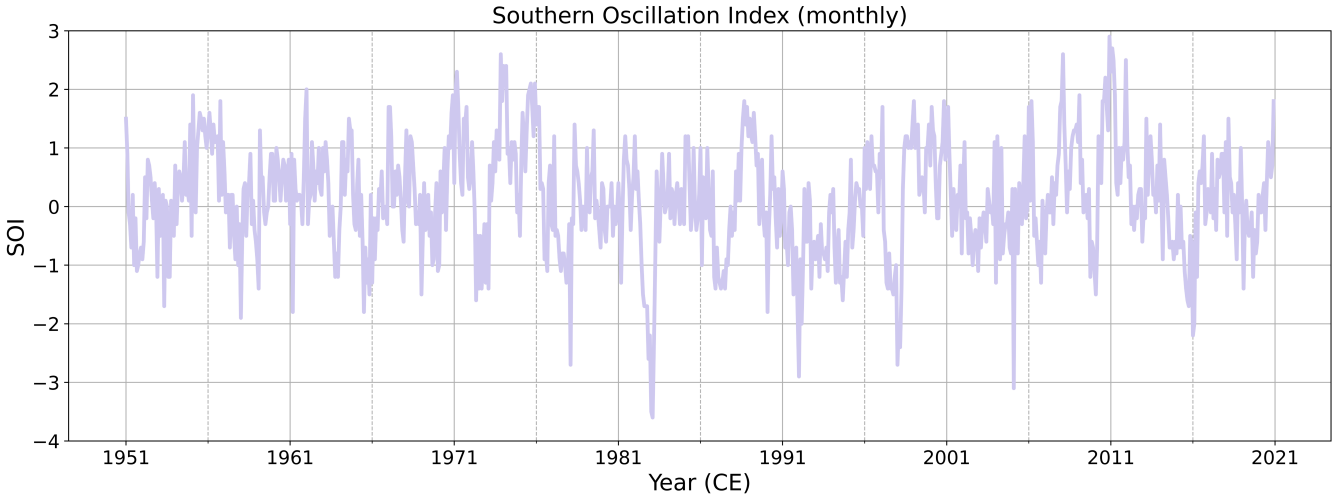

Figure 7: SOI time series derived from observations of sea level pressures at Darwin and Tahiti, provided by the US National Oceanic and Atmospheric Administration (National Centers for Environmental Information, n.d.)[25].

3 Methods

This section introduces the methods and explains the calculations used in this study. The calculations of potential temperature from temperature and surface pressure and of monthly net snow accumulation from sonic ranger height are explained in section 3.1. Section 3.2 discusses the reasoning for the use of monthly time series, the quality control applied to calculations of monthly mean values from the AWS time series, and the calculations of monthly climatological means. Section 3.3 explains the process of deriving SAM and SO indices from ERA5 MSLP data. Section 3.4 discusses this study's several applications of linear least-squares regressions and related p-values and confidence/prediction bands. The use of bias and root-mean-square-difference to assess agreement between pairs of time series are discussed in section 3.5. Finally, section 3.6 explains the processes of detrending, deseasonalizing, and standardizing data in preparation for use in empirical orthogonal function (EOF) analysis, the procedure for calculating the EOFs, and what the EOFs represent.

3.1 Potential temperature and snow accumulation

Because the measured temperature at each station is affected by the differing surface pressure at the respective sites, it is beneficial to use potential temperature. This provides a way of adjusting for the local surface pressure, allowing potential temperature to better represent the quantities of heat present and facilitate more sound comparisons between values at different elevations. For all stations, potential temperature time series were calculated from air temperature and surface pressure, as in Bolton (1980) [2]:

$$\theta(t) = T(t) \left(\frac{P_0}{P(t)} \right)^{\frac{c_p - c_v}{c_p}}$$

where $T(t)$ is air temperature and $P(t)$ is surface pressure at time t, with reference pressure $P_0 = 1014$ hPa, specific heat capacity for air at constant pressure $c_p = 1004$ J kg^{-1} K^{-1}, and specific heat capacity for air at constant volume $c_v = 717$ J kg^{-1} K^{-1}.

Because surface pressure data from AWS 12 and 13 were not available, ERA5 surface pressure at the approximate locations of each was used instead to calculate potential temperature for these stations, after such a substitution was concluded to be reasonable based on the results of comparisons between observational and ERA5 surface pressure at other sites, discussed in section 4.2.

For snow accumulation, the goal was to derive from the AWS data a time series for monthly net snow accumulation dA. From each AWS time series for sonic ranger height H, a time series for total snow accumulation A was calculated, using the first nonempty data point H_0 as the zero point, with $A(t) = H_0 - H(t)$. To provide better insight into the quantities of snow mass that accumulation represents, A was then converted from m to mm w.e. by

$$A[mm\ w.e.] = (A[m]) \cdot \rho_s$$

where the density of fresh snow is assumed constant with a value of $\rho_s = 381$ kg m^{-3}, as in Ding et al. (2020) [7]. In reality, the density of fresh snow will vary by location and over time. However, the available station data do not provide an opportunity to calculate local, time-varying estimates. Ding et al. (2020) chose the value $\rho_s = 381$ kg m^{-3} as a reasonable assumption for the local

low-accumulation conditions at Panda-1 Station [7]. Located in the katabatic region of Princess Elizabeth Land in East Antarctica, conditions at the site of Panda-1 Station are likely similar to those near AWS 8 and 9. However, the assumption of similar fresh snow density may be less sound for AWS 12 and 13, where temperatures are lower and katabatic winds are weaker.

Finally, to determine the net change in snow height for each month dA, the first available value of A for each month was subtracted from the final available value of A for that month. While A is the total net snow accumulation since the start of the time series, dA is a time series of monthly net snow accumulation. An anomalously high-magnitude value for dA of -253.14 mm w.e. in 2020 Aug. was judged to be the result of an unknown error, and was removed; the most extreme values remaining were below 90 mm w.e. in magnitude, and were considered to be realistic instances of infrequent extreme events.

3.2 Monthly mean and climatological mean calculations

Investigations in this study are focused on monthly time series, for several reasons. The AWS records are short enough that their annual time series would be limited in usefulness, and the next-largest natural choice of time scale was monthly. The READER and observational SAM and SO index time series are provided by their respective sources as monthly values, making it convenient to use monthly values in general for consistency. All ERA5 time series are available as hourly values and as monthly means; monthly values were chosen for consistency and for convenient comparison with observational values.

When calculating monthly mean values from AWS data, the condition was imposed that the data for a given month must be at least 75% complete in order to produce a mean for that month.

Although the AWS records are shorter than would be preferred for calculating climatological means (as short as approximately 5 years at AWS8, and at most nearly 23 years for AWS9), an attempt was made to approximate monthly climatological means for (potential) temperature, wind speed, and net snow accumulation from these AWS time series, taking for each month the average of its monthly values across years in the sample. The records from Amundsen-Scott and Vostok Stations, each more than 60 years in length, are used to calculate more sound monthly climatological means for (potential) temperature and wind speed at those locations. The ERA5 products for all locations cover 40 years, and are used to separately calculate monthly climatological means for (potential) temperature, wind speed, and snowfall at each location. These (approximate) monthly climatologies are discussed for the observational data in section 5.1, and for the ERA5 data in section 6.1.

3.3 Deriving SAM and SOI indices from ERA5 products

A SAM index based on ERA5 data was calculated with a process similar to that used to calculate the observation-derived SAM index (section 2.2.2) provided by the British Antarctic Survey (Marshall, n.d.)[22], with the ERA5 data allowing for the selection of data at more precise latitude coordinates and a larger number of regularly-spaced zonal points. The ERA5 products used provide monthly averages of mean sea level pressure (MSLP) at 40°S and at 65°S and for longitude values with a spacing of 2.5° in the interval $[-180°, 179.75°]$, for every month from January 1979CE to December 2020CE. At each of the two latitudes, the zonal means were calculated using all grid points in each latitude band, producing time series for zonal mean monthly mean MSLP. These

time series were each standardized (as in section 2.2.2), and the SAM index defined as

$$SAM = P^*_{40°S} - P^*_{65°S},$$

where the P^* are the standardized zonal mean monthly mean MSLP time series.

For the SOI, the ERA5 monthly mean MSLP time series were selected at 12.44°S, 130.85°E (representing Darwin, Australia), and at 17.67°S, 149.40°W (representing Tahiti). The calculations to produce the SOI were then identical to those used to produce the observation-derived SOI (section 2.2.3) provided by the US National Oceanic and Atmospheric Administration's National Centers for Environmental Information [25].

These ERA5-derived indices are compared with the observational indices in section 4.4, and are used to investigate the effects of the SAM and SO on the ERA5 variable time series in section 6.3.

3.4 Linear fits, significance, and confidence and prediction bands

For all linear least-squares regressions in this study, the two-sided p-value was calculated for a hypothesis test with the null hypothesis that the slope of the true regression line is zero, using the Wald Test with t-distribution of the test statistic (The SciPy Community, 2021)[30]. All confidence bands used are 95% pointwise confidence bands, and all prediction bands used are 95% pointwise prediction bands.

For temperature, surface pressure, and wind speed at each station site, linear least-squares regressions were used to assess the agreement between the time series for observational data and the ERA5 data. These results are discussed in section 4.

For each pair of locations the two time series for each observed variable were used to find linear least-squares regressions relating the time series at each combination of two sites. Some of these comparisons will be discussed as examples in the context of the regional climate in section 5.1 for observational data and in section 6.1 for ERA5 data.

To investigate possible trends in the monthly time series, linear least-squares regressions were calculated for each observed variable at each location as a function of time. These calculations each use an integer-valued number of years, counting backward from the most recent month available. (For example, the full monthly time series for AWS13 includes 2008 Jan. to 2016 Feb., but the linear regressions with respect to time for AWS13 time series use 2008 Mar. to 2016 Feb.) The results of these calculations are discussed in section 5.2 for the observational data and in section 6.2 for the ERA5 data.

After detrending, deseasonalizing, and standardizing each time series (section 3.6), the first step in examining the influence of the SAM and SO indices on the Plateau climate was to calculate linear least-squares regressions for each observed time series at each location versus the observation-derived SAM index, and versus the observation-derived SOI. This process was then repeated for the ERA5 time series versus the ERA5-derived SAM and SO indices. These results for the observational data and indices are discussed in section 5.3.1, and those for the ERA5 data and indices in section 6.3.1.

3.5 Assessment of agreement between observations and ERA5 products

For temperature, surface pressure, and wind speed time series at each site, the observed time series and the time series from ERA5 products were compared by calculating their bias and root-

mean-square-difference ($RMSD$):

$$bias(X) = \overline{(X_{ERA5}(t) - X_{obs}(t))},$$
$$RMSD(X) = \left(\overline{(X_{ERA5}(t) - X_{obs}(t))^2}\right)^{1/2}$$

where X represents one of the meteorological variables examined in this study and the means are taken over the set of months for which the observational and ERA5 time series overlap. Further comparison was conducted by calculating for each pair the least-squares linear regression. Similarly, for both SAM and SO indices, the observation-based and ERA5-derived time series were compared by calculating their bias, root-mean-square-difference, and least-squares linear regression. These comparisons are examined in section 4.

3.6 Empirical orthogonal function analysis

Each variable and index time series was detrended by subtracting the trend line found using linear least-squares regression versus time, then deseasonalized by subtracting from each month the climatological mean found for that time series for the month, and then standardized by subtracting from each value the mean of the time series and then dividing by the standard deviation of the time series. This produces time series that represent anomalies that are normalized with respect to the standard deviation, and with the effects of background trends and yearly cycles removed.

Empirical orthogonal function (EOF) analysis was used to examine the relations between each variable time series and the SAM and SO indices. This process requires that all parameters used in the calculations have approximately normal distributions (after detrending, deseasonalizing, and standardizing), and it was determined that all time series used in this study met this criterion. For each variable time series, the 3×3 correlation matrix was calculated for the system consisting of the time series for the variable, SAM, and SOI. The normalized eigenvectors of each correlation matrix provide the EOFs for the three-series system, and the eigenvalues describe the relative contribution of their corresponding EOFs to the total variation of the system. The three EOFs form an orthonormal basis for the three-parameter space of the variable-SAM-SOI system. The first EOF is the unique (up to sign) unit vector with respect to which the variance of the system is minimized. The second EOF is the unique (up to sign) unit vector orthogonal to the first EOF with respect to which the remaining variance is minimized. Similarly, the third EOF is the unique (up to sign) unit vector orthogonal to both the first and second EOF which minimizes the remaining variance of the system, which is uniquely determined (up to sign) by the first two EOFs.

Each EOF represents a specific combination of positive and negative couplings between the three parameters in the system, with the relative magnitudes of the vector's components indicating the relative strength of each coupling. The magnitude of the eigenvalue corresponding to an EOF indicates the strength of the influence of that particular combination of couplings, relative to the combinations represented by the other EOFs.

These calculations were performed for each observed variable time series with the observational SAM and SO indices (section 5.3.2), and again separately for each ERA5 variable time series with the ERA5-derived SAM and SO indices (section 6.3.2).

4 Comparison of observational data and ERA5 data

This section presents assessments of the agreement between observational data and ERA5 data, using linear least-squares regressions and calculations of bias and $RMSD$. In addition to temperature (section 4.1) and wind speed (4.3), surface pressure was also assessed (4.2), since calculations of potential temperature rely on the pressure time series, and because it was necessary to determine whether ERA5 surface pressure data could be substituted for the missing data from AWS 12 and 13. Comparisons between the observation-based and ERA5-derived SAM and SO indices are also examined (section 4.4), since the indices are among the central aspects of this study.

One of the factors that makes the comparisons imperfect for temperature, pressure, and wind speed is the mismatch between measurement heights and the heights of the ERA5 data. The values from ERA5 are for 2m temperature, surface pressure, and 10m wind speed. The measurement heights at Amundsen-Scott and Vostok Stations are not specified in the READER archive, and the AWS sensor heights are not consistent. The AWS masts were erected at different initial heights, and the height of each varies as snow is accumulated or removed under the mast, so that the measurement height was found to be as low as 1.00m or as high as 4.72m. Furthermore, ERA5 uses an average topographical height for each grid box, while each station makes its observations in one specific location at a topographic height that could deviate notably from the average for the ERA5 grid box it is located within. These topographic height differences are expected to have the largest effect on temperature, since there is a strong temperature gradient in the surface boundary layer. The discrepancies in surface slope, meanwhile, will affect wind speed more than temperature, since the wind is driven in large part by the slope-induced katabatic effect. A summary of the minima, maxima, means, and standard deviations of the observation heights at each AWS is shown in Table 3.

Table 3: Mean, standard deviation, minimum, and maximum of measurement heights for each AWS.

Station	mean height (m)	s.d. (m)	min. (m)	max. (m)
AWS8	2.12	0.27	1.65	2.67
AWS9	1.92	0.38	1.00	2.91
AWS12	4.07	0.21	3.67	4.72
AWS13	4.15	0.18	3.73	4.54

The ERA5-land dataset provides data for monthly total snowfall. The AWS, however, measure snow height, which is affected by precipitation and deposition, loss from drifting snow and sublimation, and compaction. While net snow accumulation can be calculated approximately from snow height by neglecting compaction (section 3.1), it is not feasible to extract snowfall from these data. While both AWS net snow accumulation and ERA5 snowfall may be useful, no meaningful direct comparison can be made between these variables; both are nonetheless included in later discussion, as parts of sections 5 and 6, respectively.

4.1 Temperature

Linear least-squares regressions found statistically significant correlations between temperature observations and ERA5 2m temperature at all locations. A large part of this is due to the time series sharing strong seasonal cycles, evidence of which can be seen in their scatterplots (examples in Figure 8) as three elongated clusters of points for winter, summer, and the transition periods. Correlations were consistently very strong, with $r > 0.99$ at every site, and $RMSD$ values ranged

from 2.6 to 5.9 °C. A summary of the p-values, r-values, and slopes of the linear fits, along with the bias and $RMSD$ values, is presented in Table 4.

The comparison at every location showed that ERA5 tends to overestimate temperature when observational values are low, and to underestimate when observational values are high. On average, the ERA5 values are higher than the observed values, indicated by the consistently positive biases. These effects could be related to the measurement height and topography, as discussed at the start of section 4, but the strength of the effects at the various sites does not appear to be related to distance inland, elevation, or surface slope. The over- and underestimation was found to be most prominent at Amundsen-Scott Station and weakest at AWS13 (both shown in Figure 8), which respectively had the largest and smallest bias and $RMSD$.

Table 4: The p-values, r-values, and slopes (m) of linear regressions, and bias and $RMSD$, for ERA5 2m temperatures versus observed temperatures, at each station site. Because the largest of the p-values was on the order of 10^{-46}, the p-values are each considered to be approximately 0.

Station	lin. reg.	bias (°C)	$RMSD$ (°C)
AWS8	$p \approx 0$ $r = 0.9948$ $m = 0.7606$	1.6	2.8
AWS9	$p \approx 0$ $r = 0.9907$ $m = 0.7532$	2.0	3.4
AWS12	$p \approx 0$ $r = 0.9903$ $m = 0.8201$	1.8	3.3
AWS13	$p \approx 0$ $r = 0.9919$ $m = 0.8488$	1.1	2.6
Amundsen-Scott	$p \approx 0$ $r = 0.9920$ $m = 0.7305$	4.7	5.9
Vostok	$p \approx 0$ $r = 0.9948$ $m = 0.7544$	3.5	5.0

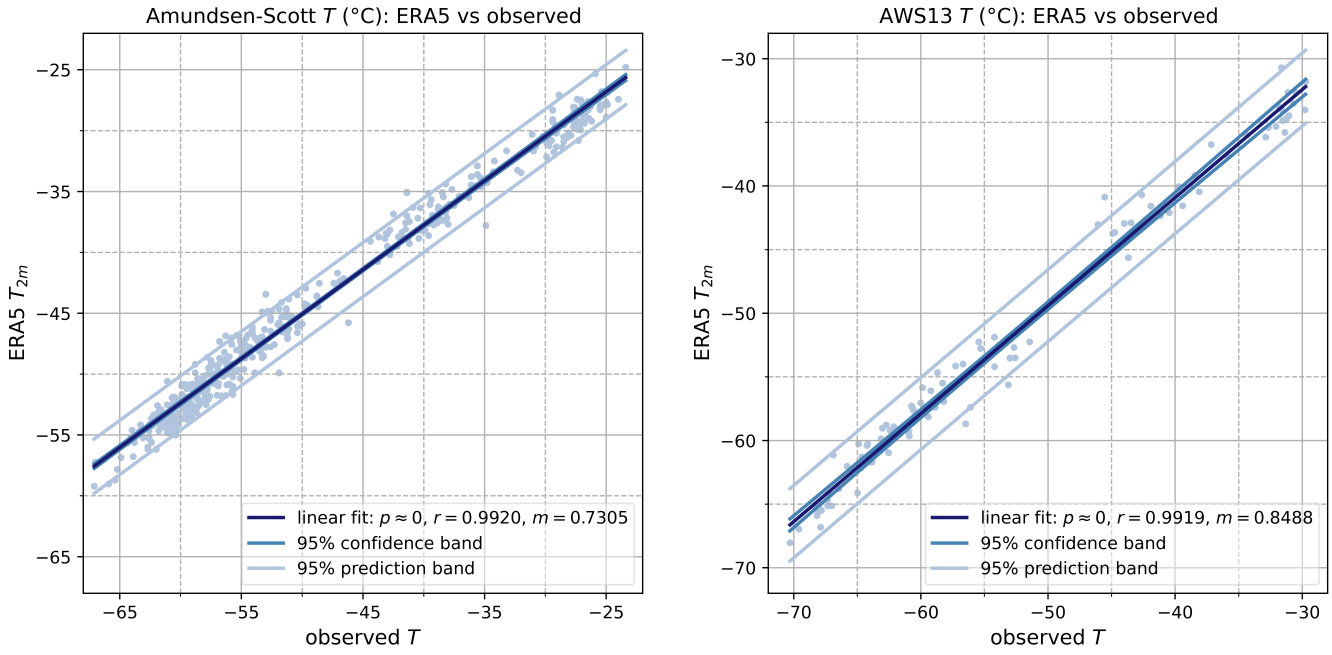

(a) (b)

Figure 8: Monthly mean ERA5 2m temperature versus observed near-surface temperature at **(a):** Amundsen-Scott Station for values within the ERA5 data period of 1981 Jan. to 2020 Dec.; **(b):** AWS13 for values within the observational period of 2008 Jan. to 2016 Feb.

4.2 Pressure

Of the four stations for which observational surface pressure data were available (AWS 8 and 9, Amundsen-Scott Station, and Vostok Station), linear least-squares regressions found statistically significant correlations between surface pressure observations and ERA5 surface pressure values at all locations. The correlations were all strong, with $r > 0.92$ at every site, and $RMSD$ values ranged from ~ 0 (within sensor error for the AWS) to 6.9 hPa. A summary of the p-values, r-values, and slopes of the linear fits, along with the bias and $RMSD$ values, is presented in Table 5.

The comparisons showed that ERA5 tends to slightly underestimate surface pressure at AWS9, particularly for higher values, and tends to overestimate at the other stations. Amundsen-Scott Station is where the most noteworthy overestimation occurs, with higher pressure values again being affected slightly more. At Vostok Station, the overestimation is very small and affects lower pressure values more, while at AWS8 the small overestimation increases for higher pressures. These differences could be at-least-partly explained by the differences in topographic height between the stations and the ERA5 grid points, suggesting that AWS9 could be positioned at a lower topographic height than the average for its ERA5 grid box, and the other stations higher than the averages for theirs. Scatter plots for the pressure comparisons at Amundsen-Scott Station and at AWS9 are shown in Figure 9.

For AWS 8 and 9, the biases and root-mean-square-differences between surface pressure from observations and from ERA5 were smaller than the measurement uncertainty of the sensors, and agreement was considered adequate to justify the use of ERA5 surface pressure values at the locations of AWS 12 and 13 to substitute for the missing pressure observations from those stations, to allow potential temperature at AWS 12 and 13 to be calculated.

Table 5: The p-values, r-values, and slopes (m) of linear regressions, and bias and $RMSD$, for ERA5 surface pressures versus observed air pressures, at each station site. Because the largest of the p-values was on the order of 10^{-28}, the p-values are each considered to be approximately 0.

Station	lin. reg.	bias (hPa)	$RMSD$ (hPa)
AWS8	$p \approx 0$ $r = 0.9673$ $m = 1.055$	~ 0	~ 0
AWS9	$p \approx 0$ $r = 0.9269$ $m = 0.9139$	~ 0	~ 0
Amundsen-Scott	$p \approx 0$ $r = 0.9949$ $m = 0.9489$	6.8	6.9
Vostok	$p \approx 0$ $r = 0.9807$ $m = 0.9818$	0.8	1.5

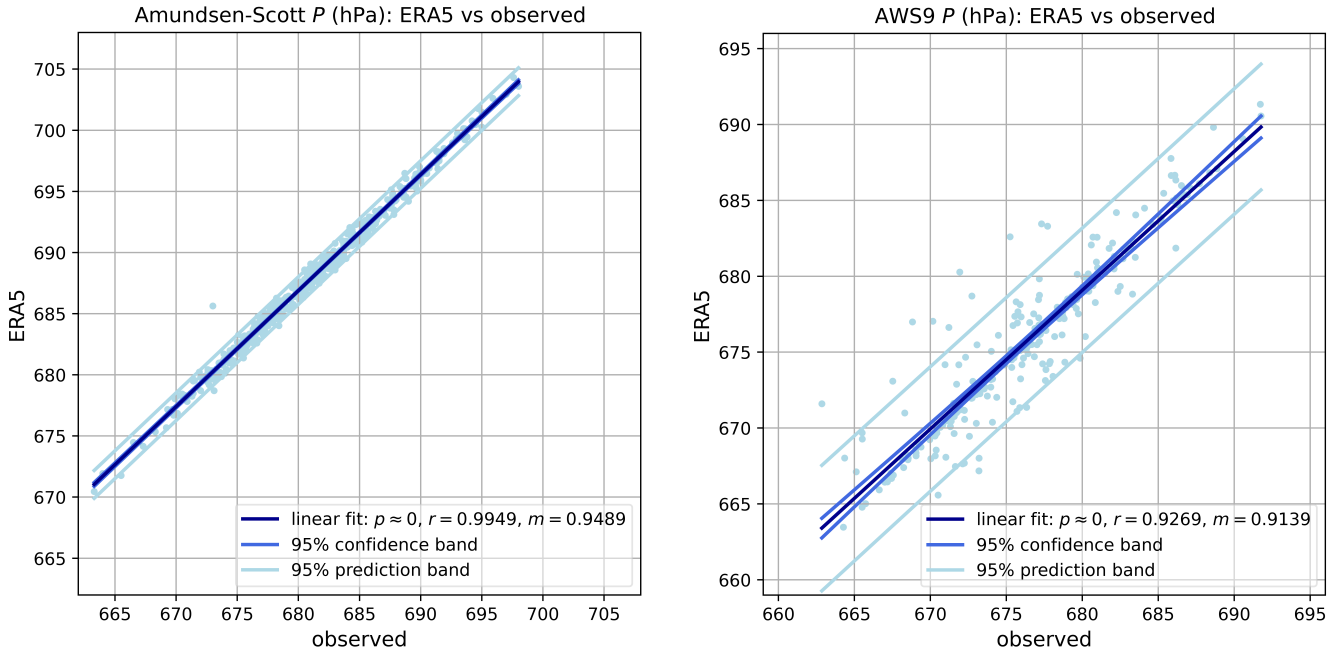

(a) (b)

Figure 9: Monthly mean ERA5 surface pressure versus observed surface pressure at **(a):** Amundsen-Scott Station for values within the ERA5 data period of 1981 Jan. to 2020 Dec.; **(b):** AWS9 for values within the observational period of 1998 Jan. to 2020 Sep.

4.3 Wind speed

The wind speed data are not as directly comparable as those for temperature and surface pressure, for several reasons. As discussed at the start of section 4, the difference in measurement height is one such factor, so that the observed values measured closer to the surface are expected to be lower than the ERA5 values from higher above. Another of these factors is the local topography, which can have a large influence on wind in particular, since the katabatic flow is dependent upon the local surface slope, and since other surface features can act to direct the flow of air near the surface. Additionally, because wind exhibits large variance on small spatial scales, and because the resolution of ERA5 limits the precision with which the location of ERA5 data can match the location of a station, the exactness of the comparison is further reduced.

Of the five stations for which observational wind speed data were available (all except AWS13), linear least-squares regressions found statistically significant correlations between wind speed observations and ERA5 10m wind speed at all locations. With the exception of Vostok Station, all sites had $r > 0.6$. The $RMSD$ values ranged from 0.7 to 1.1 m s^{-1}, and the signs of the biases were inconsistent. A summary of the p-values, r-values, and slopes of the linear fits, along with the bias and $RMSD$ values, is presented in Table 6.

Table 6: The p-values, r-values, and slopes (m) of linear regressions, and bias and $RMSD$, for ERA5 10m wind speeds versus observed wind speeds, at each station site. Because the largest of the p-values was on the order of 10^{-8}, the p-values are each considered to be approximately 0.

Station	lin. reg.	bias (m s^{-1})	$RMSD$ (m s^{-1})
AWS8	$p \approx 0$ $r = 0.7266$ $m = 0.7473$	-0.2	0.8
AWS9	$p \approx 0$ $r = 0.7352$ $m = 0.9457$	0.2	0.7
AWS12	$p \approx 0$ $r = 0.6400$ $m = 1.037$	-0.5	0.8
Amundsen-Scott	$p \approx 0$ $r = 0.7413$ $m = 0.8070$	0.1	0.7
Vostok	$p \approx 0$ $r = 0.2532$ $m = 0.2037$	-0.5	1.1

The findings of these wind speed comparisons are quite inconsistent. On average, ERA5 10m wind speed tends to be higher than observed wind speed at AWS9, very slightly higher than observations at Amundsen-Scott Station, and lower than observed values at Vostok Station and AWS 8 and 12. At Amundsen-Scott Station, ERA 10m wind speeds tend to be higher than the observations for lower values, and lower than observations for higher values. The regression slopes range from 0.2037 at Vostok Station to 1.037 at AWS12, with slopes within ± 0.06 of 1 found at AWS 9 and 12, and within ± 0.035 of 0.78 at AWS8 and Amundsen-Scott Station. It is possible that differences in surface slopes could be a cause of these inconsistencies, with the slope having a larger effect on the lower observations than on the 10m ERA5 wind speeds; verifying or falsifying this would require specific information on surface slopes at each measurement site, which is not provided by the datasets used in this study. Scatter plots for the wind speed comparisons at AWS9 and Amundsen-Scott Station are shown in Figure 10.

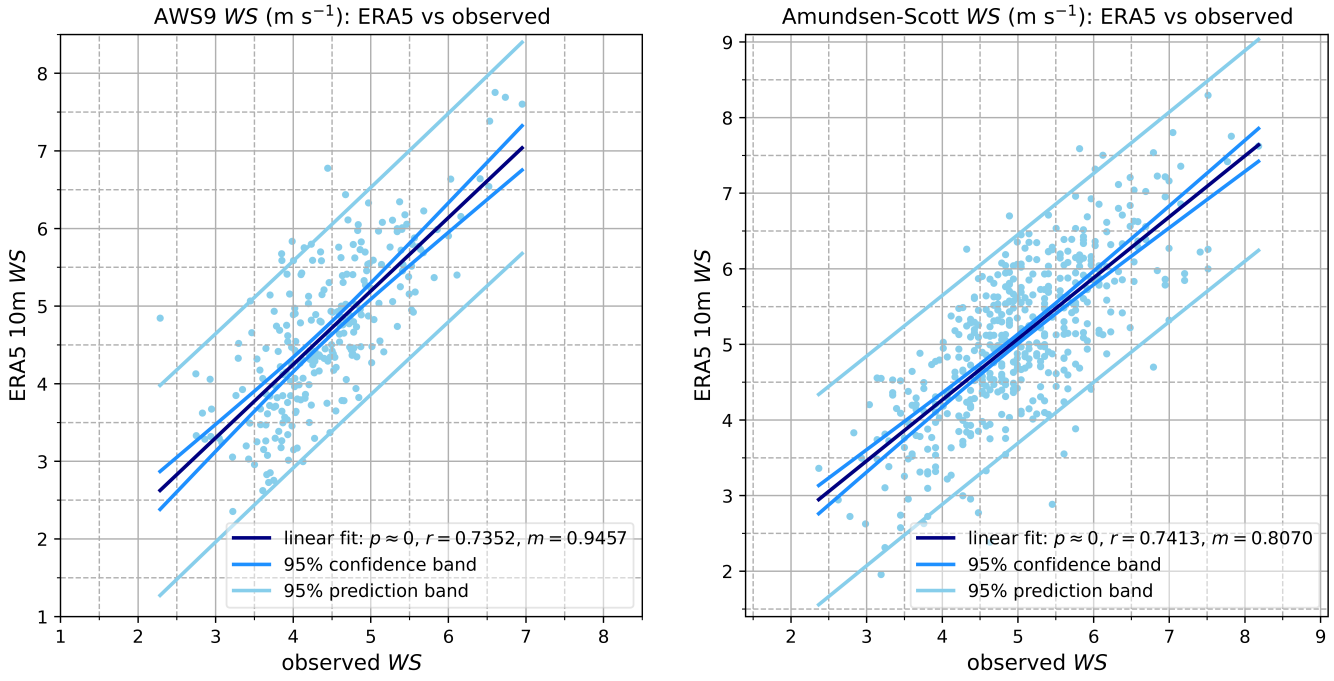

(a) (b)

Figure 10: Monthly mean ERA5 10m wind speed versus observed near-surface wind speed at
(a): AWS9 for values within the observational period of 1998 Jan. to 2020 Sep.;
(b): Amundsen-Scott Station for values within the ERA5 data period of 1981 Jan. to 2020 Dec.

4.4 SAM and SO indices

SAM index

A significant correlation was found between the ERA5-derived and observation-based SAM index, with $p \approx 0$, $r = 0.7133$, and a fit line slope of $m = 0.7454$; the $RMSD$ of the two versions of the index is 1.377. A scatter plot comparing the two is shown in Figure 11a. The ERA5 version of the index is an average of 0.2666 lower than the observational index, and tends to have values of lower magnitude for any given time, possibly due to being less sensitive to extreme events at any one location. Considering that the two versions of the index are not perfectly comparable because of their differing calculation methods, this is a reasonable degree of agreement. The observation-based index was calculated by approximating zonal means using six measurement stations near 40°S and six near 65°S, with irregular zonal spacing. The ERA5 dataset, meanwhile, provides for each latitude band a total of 3600 regularly-spaced zonal points from which the zonal means were calculated. Because of this difference, climatological pressure patterns (such as the SAM itself, ENSO, or other modes) are likely to have larger impacts on the observational SAM index, due to local anomalies at individual measurement sites having a larger weight in the calculation.

SO index

Because the SOI derived from ERA5 products was calculated using a very similar method to the observational SOI, the two share a stronger similarity than do the two SAM indices. A significant correlation was found between the ERA5-derived and observation-based SOI, with $p \approx 0$, $r = 0.8914$, and a fit line slope of $m = 0.9351$; the $RMSD$ of the two versions of the index is 0.4582. A scatter plot comparing the two is shown in Figure 11b. The ERA5 version of the index is an average of 0.02635 lower than the observational index, and tends to have values of slightly lower magnitude for any given time. A possible cause of differences is that the index might be sensitive to small differences in the coordinates used to select locations for the ERA5 data.

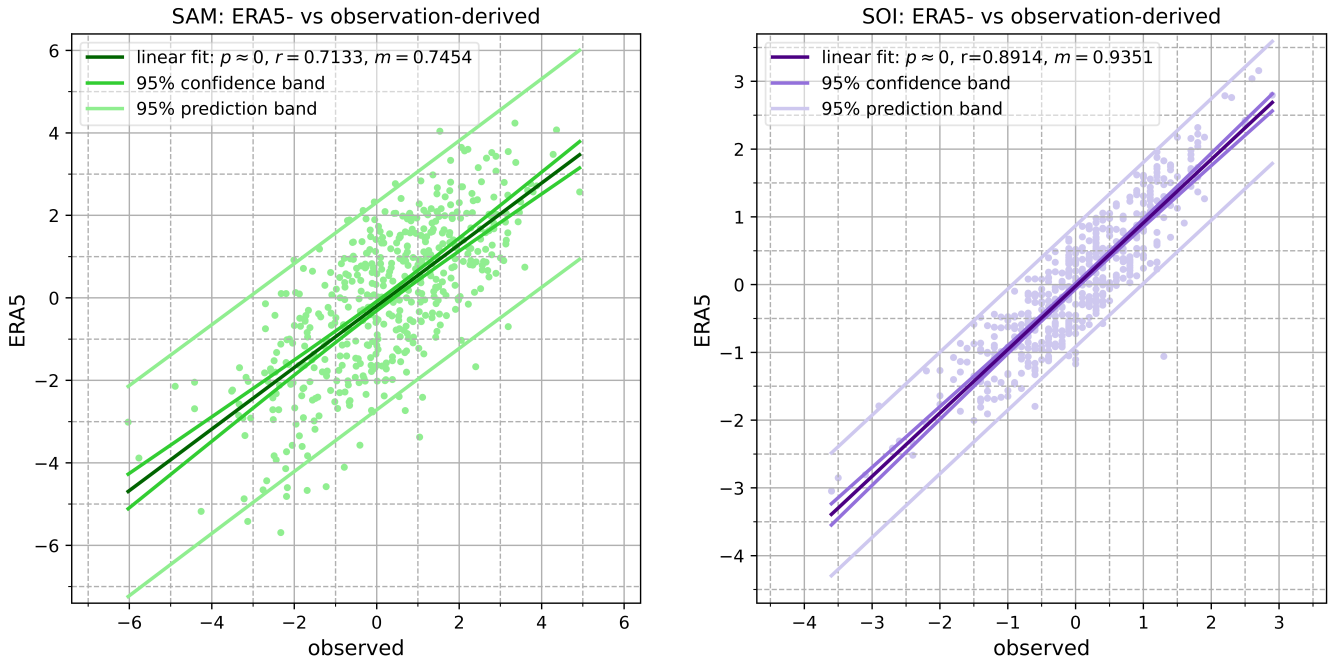

(a) (b)

Figure 11: **(a):** SAM index calculated from ERA5 monthly average mean sea level pressure (section 3.3) versus the SAM index calculated from observed values (section 2.2.2), 1979 Jan. to 2020 Dec.; **(b):** SOI calculated from ERA5 monthly average mean sea level pressure (section 3.3) versus the SOI calculated from observed values (section 2.2.3), 1979 Jan. to 2020 Dec.

5 Investigation of observational data

This section presents findings for the observational data from AWS 8, 9, 12, and 13, Amundsen-Scott Station, and Vostok Station (introduced in section 2.1), and the observation-derived SAM and SOI (sections 2.2.1 and 2.2.2, respectively). The climatology of the Plateau is explored first, using monthly climatological means and comparisons of conditions between sites (section 5.1). Then, the monthly time series and their linear trends with respect to time are examined (section 5.2), followed by investigations of the influences from the SAM and SO indices (section 5.3) using linear regressions (5.3.1) and EOF analysis (5.3.2).

Due to missing data from AWS13, all investigation of observed wind speed is applied to five stations: AWS 8, 9, and 12, Amundsen-Scott Station, and Vostok Station. Similarly, because the READER archive does not include measures of snow accumulation at Amundsen-Scott and Vostok Stations, all investigation of monthly net snow accumulation is limited to AWS 8, 9, 12, and 13.

5.1 Plateau climatology

Despite the relatively short durations of the AWS records, they produce approximate (potential) temperature climatologies that closely resemble the patterns of those for Amundsen-Scott and Vostok Stations. In accordance with the expected seasonal cycle on the Plateau, the highest temperatures occur in December and January, with more extreme cold temperatures from April to September, and the lowest found in July or August. Most sites clearly display the "coreless" winters typical to the region, with the climatologies showing almost uniform temperatures throughout the Antarctic winter. During the transition periods between January and April and between September and December, changes in mean temperature from each month to the next are often around $\pm 10°C$, with the largest differences typically found farther inland, since these sites are at higher elevations, where the thin atmosphere enables stronger radiative cooling and the smaller surface slopes allow the temperature inversion to remain more stable.

While the maximum average monthly potential temperature is within $\pm 5°C$ of $0°C$ at all stations, the minima vary by location. AWS8 is found to be the warmest site, followed by AWS9, both of which are notably not as far inland as the other four stations; both have minimum potential tempeatures of around $-23°C$ to $-25°C$. The remaining four stations each have minimum potential temeratures of approximately $-30°C$ to $-36°C$. This indicates that even adjusting for elevation, locations farther inland on the Plateau experience more extreme cold during winter. The coldest site is Vostok Station, since the surrounding depression in the ice and relatively flat surface result in a more stable atmospheric boundary layer that loses more heat to radiative cooling during the polar night. The remaining three sites are slightly warmer than Vostok Station. These same comparisons also hold for the actual temperature. Climatologies for AWS9 and Vostok Station are shown as selected examples in Figure 12.

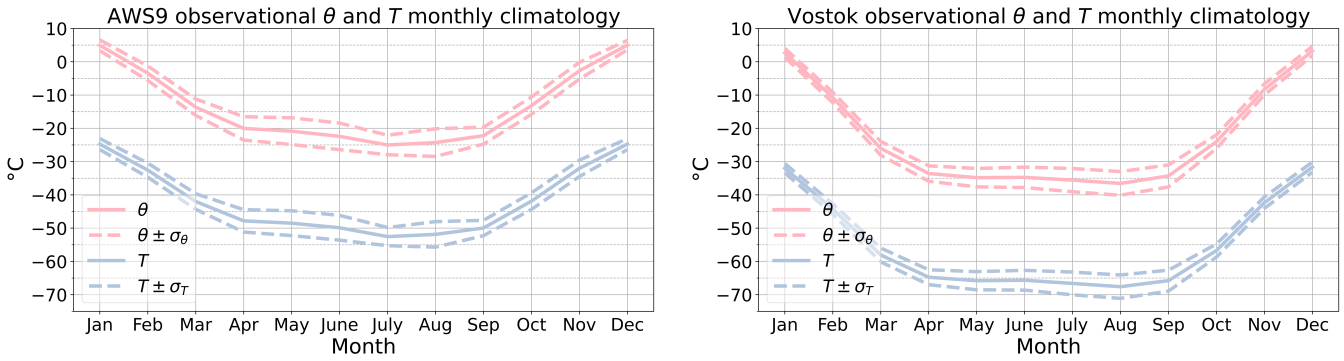

(a) (b)

Figure 12: Selected examples of (approximated) monthly climatologies for (potential) temperature, with their respective standard deviation bands, at **(a):** AWS9 (1998 Jan. to 2020 Sep.); **(b):** Vostok Station (1958 Jan. to 2020 Dec.).

The yearly cycle and spatial pattern are also evident when using scatter plots and linear regressions to compare the potential temperature time series between pairs of stations (examples shown in Figure 13). The prominent seasonal cycle results in strong correlations between potential temperature at every pair of sites, and each scatter plot contains three distinct clusters of points for the winter, summer, and transitionary months. Values at AWS 8 and 9 are very similar, as are those at AWS 12 and 13 (Figure 13a), since each of these pairs is in close proximity and shares similar conditions. All locations share quite similar values during summer, while values in winter are lower farther inland (e.g. AWS9 compared to Amundsen-Scott Station, Figure 13b), and at higher elevation (e.g. Amundsen-Scott Station compared to AWS13, Figure 13c). The lowest winter potential temperatures are found at Vostok Station (compared with AWS13 in Figure 13d).

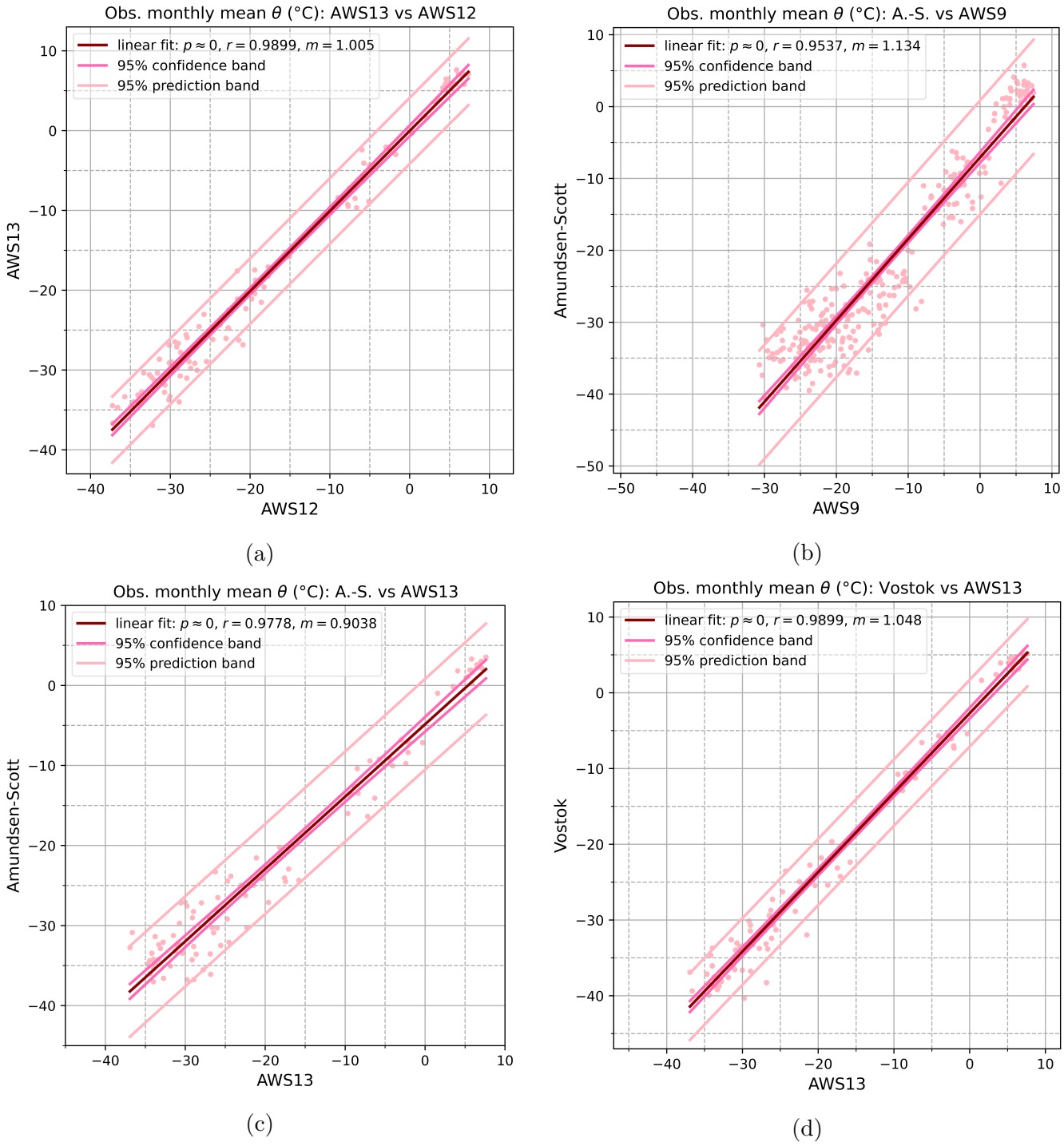

Figure 13: Scatter plots with linear regressions comparing monthly mean potential temperature time series at **(a):** AWS 12 and 13 (2008 Jan. to 2016 Feb.); **(b):** AWS9 and Amundsen-Scott Station (1998 Jan. to 2020 Sep.); **(c):** AWS13 and Amundsen-Scott Station (2008 Jan. to 2016 Feb.); **(d):** AWS13 and Vostok Station (2008 Jan. to 2016 Feb.).

The (approximated) wind speed climatologies broadly follow the expected pattern of higher speeds during colder months and lower speeds during warmer months. Amundsen-Scott Station adheres most closely to this pattern, with wind speeds at the other four stations each found to lower around June or July before rising again around September or October. For Vostok Station, this might be explained by its location in a relatively flat depression in the ice sheet, allowing a more stable boundary layer to form during winter; for the AWS sites, this could be because of the shorter AWS records not accurately representing the climatological averages that could be found for longer time intervals. Although lowest average wind speeds are consistently found in either December or January, there is no agreement on the month of highest wind speeds, with peaks found in March (Vostok), May (AWS12), July (Amundsen-Scott), September (AWS8), and October (AWS9). The observed spatial variability could also be due in part to the semi-annual oscillation, another large-scale atmospheric flow pattern known to impact near-surface wind speeds in the Antarctic (van den Broeke, 2000)[35], which is not examined in this study.

The highest average monthly wind speed among the stations is 6.416 m s^{-1}, found at AWS8 in September, which is likely due to its location at a relatively low altitude and in the katabatic zone, where the surface boundary layer is less stable during the colder months, during which the temperature inversion on the upper Plateau is stronger and more katabatic wind occurs at this site. The lowest average wind speed, 3.764 m s^{-1}, is also found at AWS8, in January, possibly due to the relative lack of katabatic wind in the summer months, when the temperature inversion on the upper Plateau is relatively weak. The local conditions at AWS8, in a lower region of the Plateau, are also such that the surface radiation fluxes are nearly in balance, meaning that less radiative cooling occurs and the local temperature inversion is weaker. This weaker temperature inversion helps facilitate stronger katabatic flow from higher on the Plateau during winter, and a weaker locally-driven katabatic flow during summer.

Climatologies for AWS9 and Amundsen-Scott Station are shown as selected examples in Figure 14.

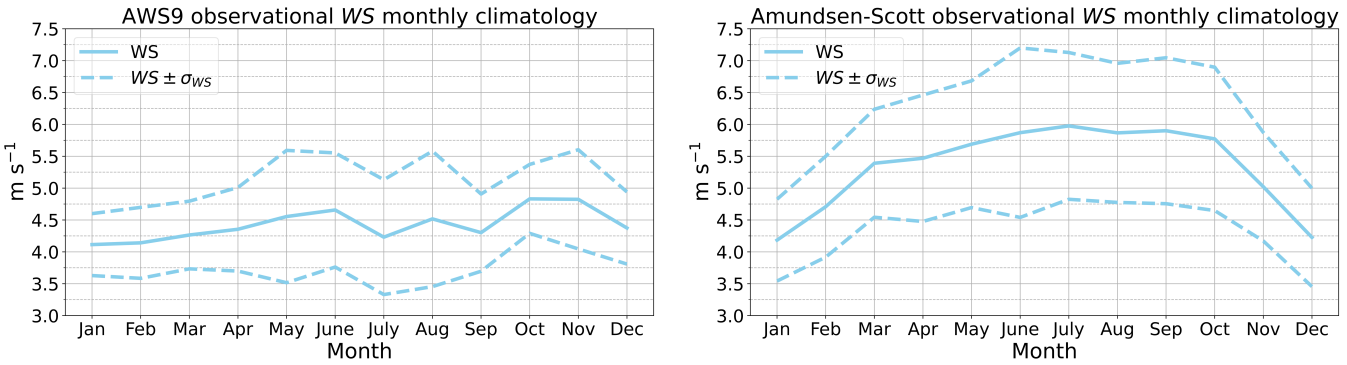

(a) (b)

Figure 14: Selected examples of monthly climatologies for wind speed, with their respective standard deviation bands, at **(a):** AWS9 (1998 Jan. to 2020 Sep.); **(b):** Amundsen-Scott Station (1957 Jan. to 2020 Dec.).

The scatter plots and linear regressions comparing monthly mean wind speed between stations are less informative than those for potential temperature. Though some linear regressions were found

with $p < 0.05$, the scatters are large and the correlations are weak. These plots and regressions give little-to-no indication of spatial patterns or of any yearly cycle being shared between locations, likely because of the high variability of wind speeds in space and time obscuring any such patterns. The scatter plot for the air of stations with the highest correlation between wind speeds was AWS 8 and 9 (Figure 15a). A more typical example is the case of Amundsen-Scott and Vostok Stations (Figure 15b).

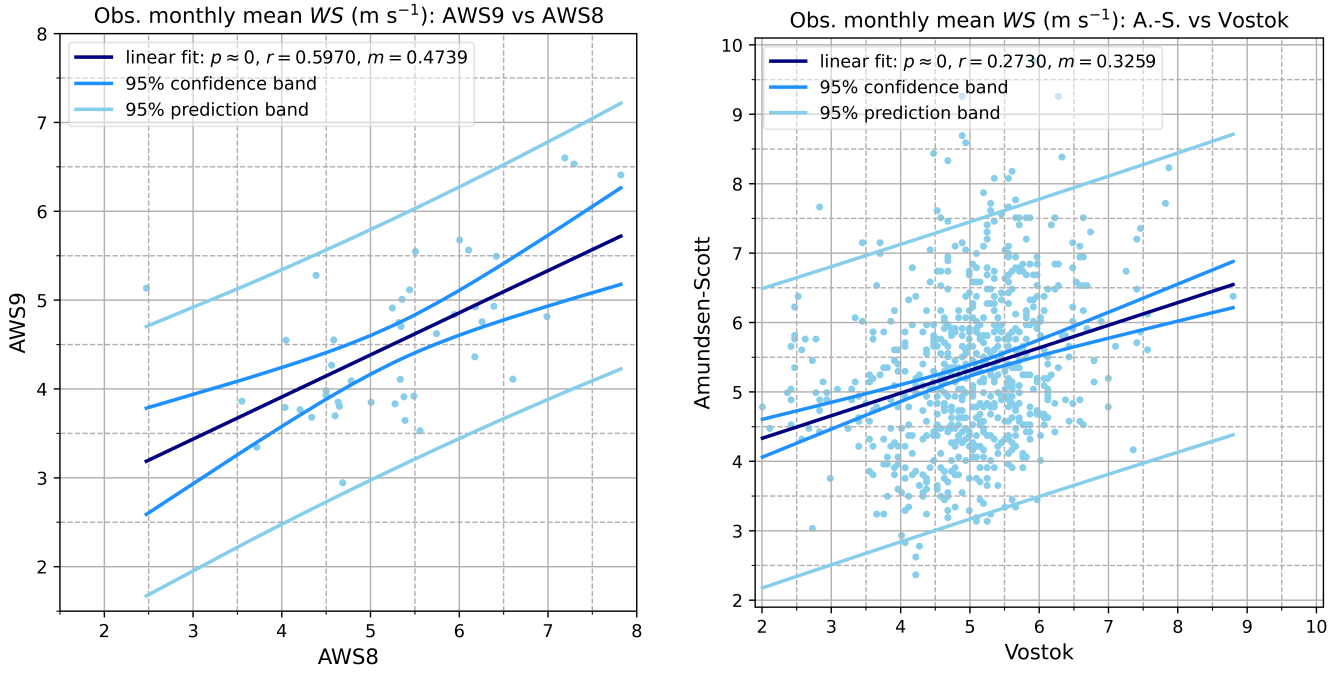

(a) (b)

Figure 15: Example scatter plot with linear regression comparing monthly mean wind speed at **(a):** AWS 8 and 9 (1998 Feb. to 2002 Dec.); **(b):** Amundsen-Scott and Vostok Stations (1958 Jan. to 2020 Dec.).

The approximated monthly snow accumulation climatologies share no clear pattern between the four; although the climatologies for AWS 12 and 13 show some resemblance, those for AWS 8 and 9 share this resemblance only from approximately May to September. Several factors contribute to these results being varied and somewhat unclear. Colder months are expected to experience reduced available moisture, but increased also snow drift due to the stronger katabatic winds, resulting both in less snowfall and in more transfer of snow from place to place. Additionally, since the Plateau is a very moisture-poor polar desert where little sublimation occurs to return moisture to the air locally, snow accumulation is ultimately dependent on advection of moisture from lower latitudes. Because of this dependence on advected moisture and the low temperatures that quickly remove most of it from the atmosphere, most precipitation on the Plateau occurs during a small number of irregular events. Climatology calculations are thus heavily affected by when the largest of these events happen to occur. With these factors taken in aggregate, it is therefore unsurprising that the climatologies have large monthly standard deviations, and show no clear connection between average monthly net accumulation and time of year. However, some general statements about

maxima and minima can be made.

In general, the four climatologies each have a local maximum in the February-April period as falling temperatures are acting to reduce the moisture capacity of the air, one in either June or July as temperatures typically reach their lowest values of the year and katabatic winds are strong. Local maxima are also consistently found in either September or October as the Antarctic winter is ending, beginning to weaken meridional temperature and pressure gradients, resulting in weaker circumpolar currents and more exchange of air masses with lower latitudes, so that more moisture is carried to the Plateau from lower latitudes. This latter maximum is the absolute maximum for all climatologies except in the case of AWS9 (which has its absolute maximum in April).

Each also has at least one local minimum in the October-March period, with those for AWS8 and 9 each having several months of low net accumulation within this period. Each of the four climatologies show additional local minima in May, following the large amounts of accumulation during the transition to winter, and in either July or August as the long Antarctic winter enters its second half and very little moisture remains in the air. The absolute minimum occurs in either July or August for all except AWS8 (which has its absolute minimum in February).

Contrary to the expectations that net snow accumulation would be reduced at higher elevations and farther inland, the approximated climatologies show no clear indication of a spatial pattern. This is possibly attributable to the shortness of the AWS records, or could in part be a side-effect of the imprecision that comes with the fact that net snow accumulation represents a combination of precipitation, deposition, drifting snow, and sublimation, without directly measuring any one of these (as discussed in the final introductory paragraph of section 4).

Climatologies for AWS 9 and 12 are shown as examples in Figure 16.

Changes in precipitation and surface mass balance in Antarctica are of particular interest in the context of ongoing anthropogenic climate changes and sea level rise. The recent upward trend in the SAM is expected to result in reduced precipitation over much of the Antarctic continent. A study by Medley and Thomas (2019) found that snow accumulation has indeed been decreasing in recent decades over much of Antarctica and most of the Plateau, and that these trends are largely attributable to the SAM [23]. However, they also found that snow accumulation in other regions of Antarctica, especially the peninsula, has increased, and that these increases are not as strongly related to the SAM (Medley and Thomas, 2019)[23]. The net result has been an average increase in snow accumulation over Antarctica, which has thus far been helping to mitigating sea level rise (Medley and Thomas, 2019)[23].

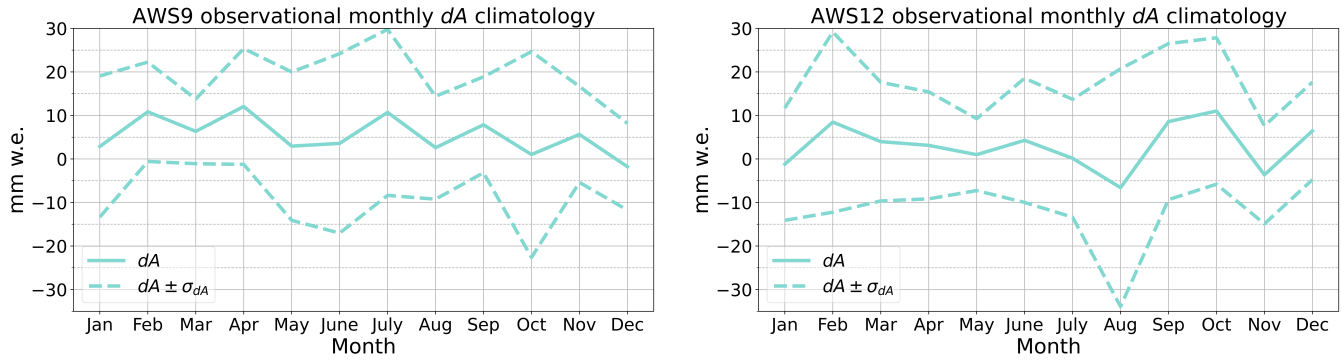

(a) (b)

Figure 16: Selected examples of monthly climatologies for monthly net snow accumulation, with their respective standard deviation bands, at **(a):** AWS9 (1998 Jan. to 2020 Sep.); **(b):** AWS12 (2008 Jan. to 2016 Feb.).

Comparisons of monthly net snow accumulation between AWS sites found only one correlation with $p < 0.05$, for AWS 9 and 12 (Figure 17). AWS9 experiences slightly higher accumulation on average, as its position lower on the Plateau would suggest. AWS12, however, experiences a larger number of more extreme accumulation and removal events, suggesting that snow accumulation higher on the Plateau tends to be less varied, with the exceptions of these uncommon extreme events. These events are likely caused by a combination of anomalously high or low temperatures, wind speeds, and moisture fluxes.

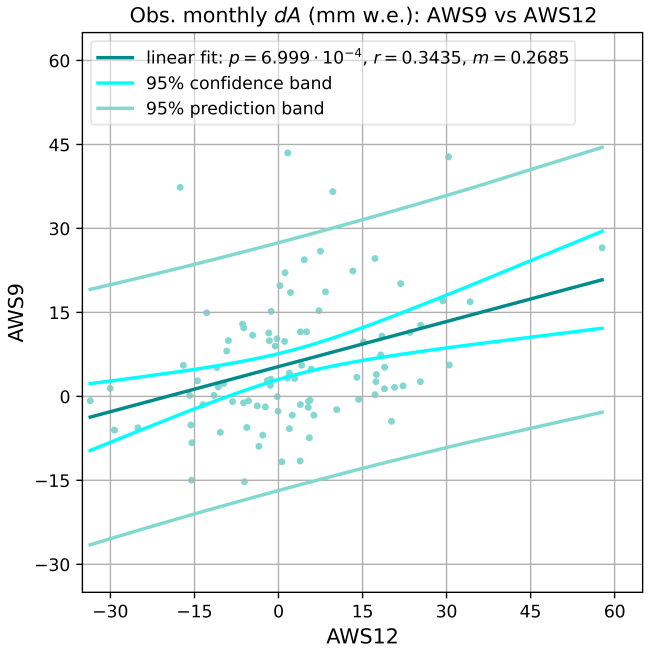

Figure 17: Scatter plot with linear regression comparing monthly net snow accumulation at AWS 9 and 12 (2008 Jan. to 2016 Feb.).

5.2 Monthly mean time series, and linear trends

The monthly mean time series for temperature and potential temperature at every station display the clear yearly cycle that the climatologies suggest should be present, with short peaks in the summers, long winters, and rapid transition periods between. The time series for monthly mean temperature and potential temperature at AWS13 are shown in Figure 18 as examples.

Linear least-squares regression detected no trends with respect to time with $p < 0.05$ for temperature or potential temperature at any site, and thus the fit lines are not shown in Figure 18. This could be due to the strong seasonal cycles obscuring possible trends, but also is consistent with the common findings of no statistically significant trend on the Plateau.

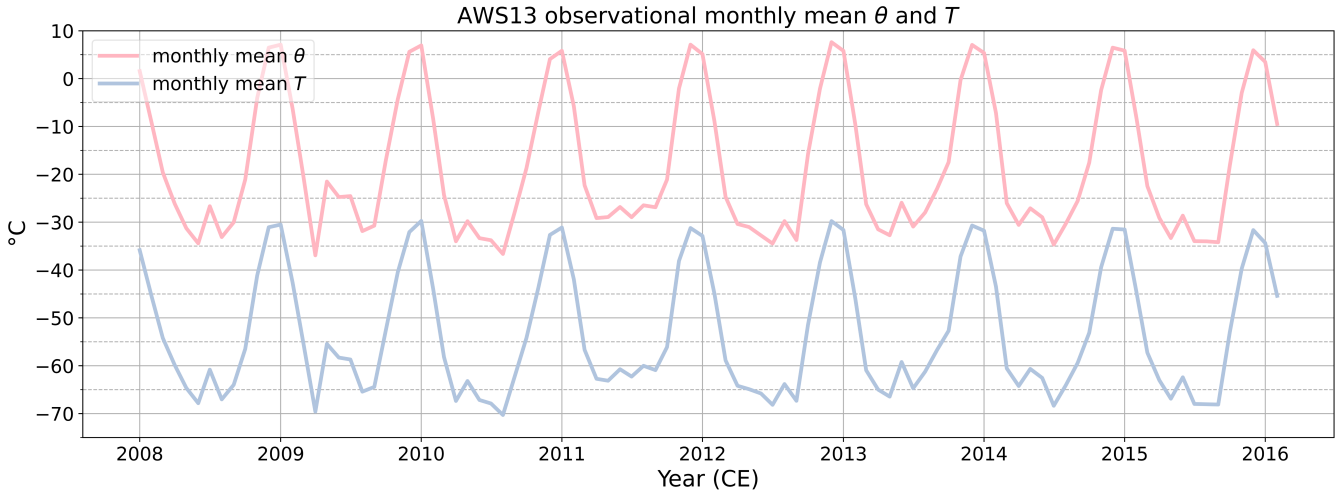

Figure 18: AWS13 monthly mean temperature and potential temperature time series (2008 Jan. to 2016 Feb.).

Because the monthly mean wind speeds at all stations exhibit noticeably more variabilitythan (potential) temperature, the yearly cycles suggested by the climatologies can be difficult to visually identify in the monthly mean time series for the stations. The simpler pattern of the climatology at Amundsen-Scott Station (Figure 14b) is relatively easy to identify in the monthly mean time series, with the yearly peaks being present for most years (Figure 19).

Linear least-squares regressions detected wind speed trends with respect to time with $p < 0.05$ only at AWS12, Amundsen-Scott Station, and Vostok Station. These three

Table 7: p-values, r-values, and slopes (m) of linear regressions for wind speed versus time, shown for those with $p < 0.05$. For Amundsen-Scott and Vostok Stations, the p-values were on the order of 10^{-13} at most, and so are considered to be approximately 0.

Station	Wind speed vs time
AWS12	$p = 0.02114$ $r = -0.2376$ $m = -0.4932$ m s^{-1} per decade
Amundsen-Scott	$p \approx 0$ $r = -0.3305$ $m = -0.2093$ m s^{-1} per decade
Vostok	$p \approx 0$ $r = -0.2692$ $m = -0.1391$ m s^{-1} per decade

trends are all toward slower winds over time, consistent with the lower wind speeds expected on the Plateau in response to the upward trend in the SAM in recent decades (Marshall, 2003; Schneider et al., 2012b; van den Broeke and van Lipzig, 2004)[17][29][36]. The strongest trend was found at AWS12, with a slope of -0.4932 m s^{-1} per decade ($p = 0.02114$), and the weakest at Vostok Station, with a slope of -0.1391 m s^{-1} per decade ($p \approx 0$). The trend line for monthly mean wind speed at Amundsen-Scott Station is shown together with the time series in Figure 19, and a summary of the p-values, r-values, and slopes of the $p < 0.05$ linear regressions is presented in Table 7.

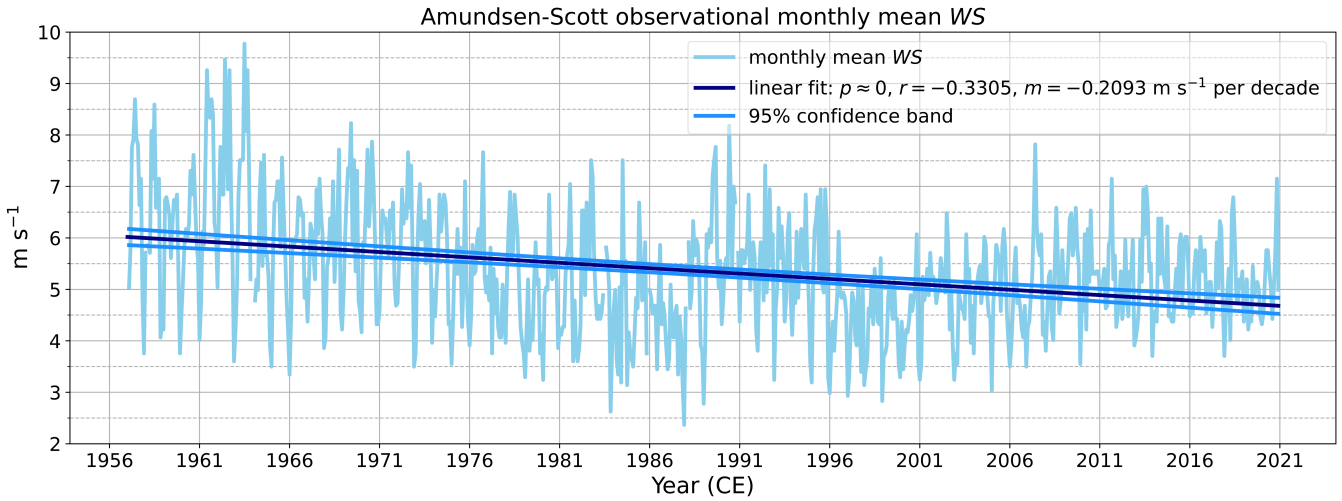

Figure 19: Amundsen-Scott Station monthly mean wind speed time series (1957 Jan. to 2020 Dec.).

Linear least-squares regression detected no trends with respect to time with $p < 0.05$ for monthly net snow accumulation at any site. This suggests that no statistically significant changes in monthly net snow accumulation are occurring over time at these Plateau sites. The monthly net snow accumulation time series at AWS12 is shown in Figure 20 as an example, where positive values indicate months which experienced more total addition of snow than removal, and negative values represent a net loss of snow.

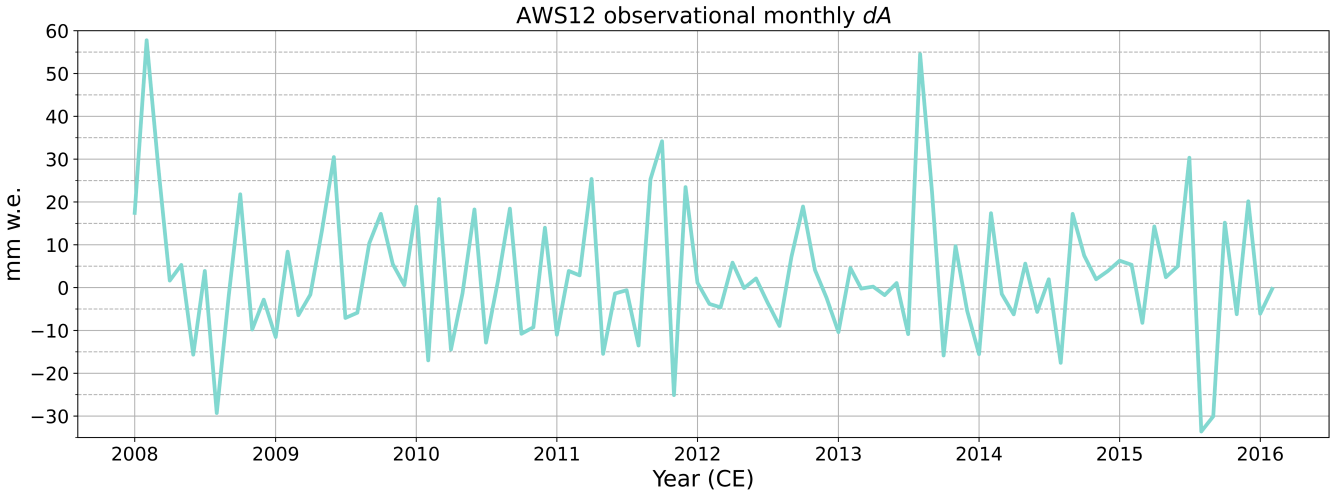

Figure 20: AWS12 monthly net snow accumulation time series (2008 Jan. to 2016 Feb.).

5.3 Influences of the SAM and SO indices

After each time series for (potential) temperature, wind speed, net snow accumulation, SAM, and SOI had been detrended, deseasonalized, and standardized, associations between the meteorological variables and each index were investigated, first using linear least-squares regressions, and then with EOF analysis.

5.3.1 Linear regressions versus the indices

SAM index

For the SAM, linear regressions with $p < 0.05$ were found for (potential) temperature at all sites except AWS8, for wind speed only at AWS9 and Amundsen-Scott Station, and for net snow accumulation only at AWS9. This suggests that the SAM has a fairly consistently detectable effect on (potential) temperatures on the Plateau, while the influence on wind speed and snow accumulation appears to be more limited or difficult to detect. A summary of the p-values, r-values, and slopes of these linear regressions is presented in Table 8.

For (potential) temperature versus the SAM, the linear regressions consistently show the expected negative correlations, indicating that positive SAM phase tends to correspond to lower (potential) temperatures on the Plateau. Of the five sites with statistically significant fits, the strength of the correlations consistently increases for sites farther inland, likely due to the higher-elevation experiencing more radiative cooling, resulting in higher sensitivity to changes in advection of heat toward the inland, and therefore higher sensitivity to the SAM because of its influence on advection patterns. Both temperature and potential temperature had the weakest correlation at AWS9 and the strongest correlation at AWS13. Correlations at all locations are stronger for temperature than for potential temperature, possibly indicating a weaker influence of the SAM on the surface pressure than on the temperature near the surface; this possibility could be examined by conducting a similar investigation for surface pressure as for the other variables in this study, using observations from the same stations. Scatter plots of the data at these sites versus SAM are

presented as examples in Figure 21.

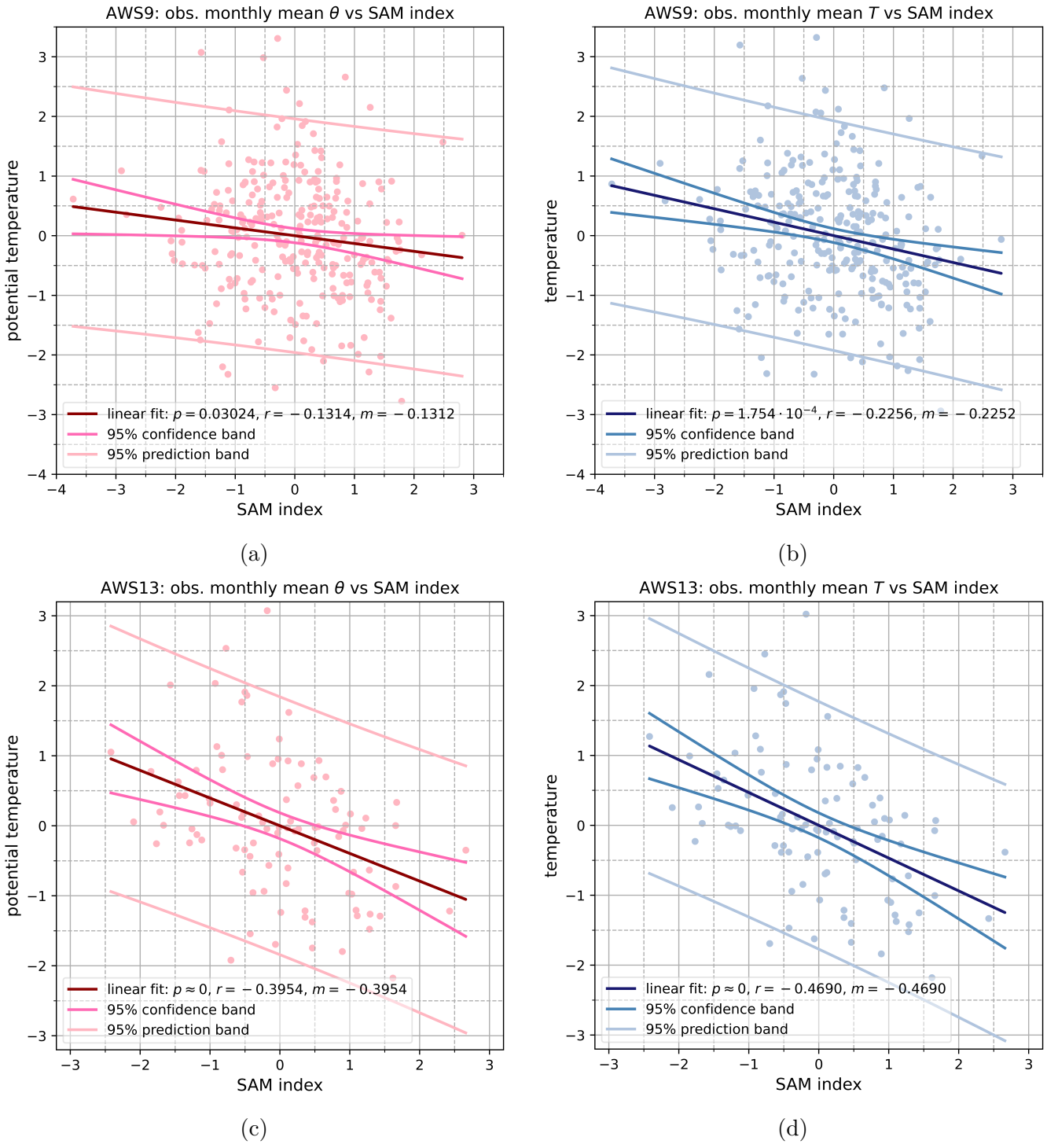

Figure 21: Monthly mean potential temperature (a and c) and temperature (b and d) versus the SAM index with linear regressions at **(a) and (b):** AWS9 (1998 Jan. to 2020 Sep.); **(c) and (d):** AWS13 (2008 Jan. to 2016 Feb.).

Despite wind speeds versus the SAM index having a large amount of scattering, statistically significant ($p < 0.05$) correlations were found at AWS9 ($p = 0.03854$) and Amundsen-Scott Station ($p = 3.987 \cdot 10^{-3}$). This suggests that either the SAM does not affect wind speed at all sites, or that its influence has not been detected consistently in these datasets by these methods. The fits at AWS9 and Amundsen-Scott Station found negative correlations, consistent with previous studies (Schneider et al., 2012b; van den Broeke and van Lipzig, 2004)[29][36], with the correlation – and the effect of the SAM on wind speed – being slightly weaker at Amundsen-Scott Station than at AWS9. Scatter plots of the data at these sites versus SAM are presented as examples in Figure 22.

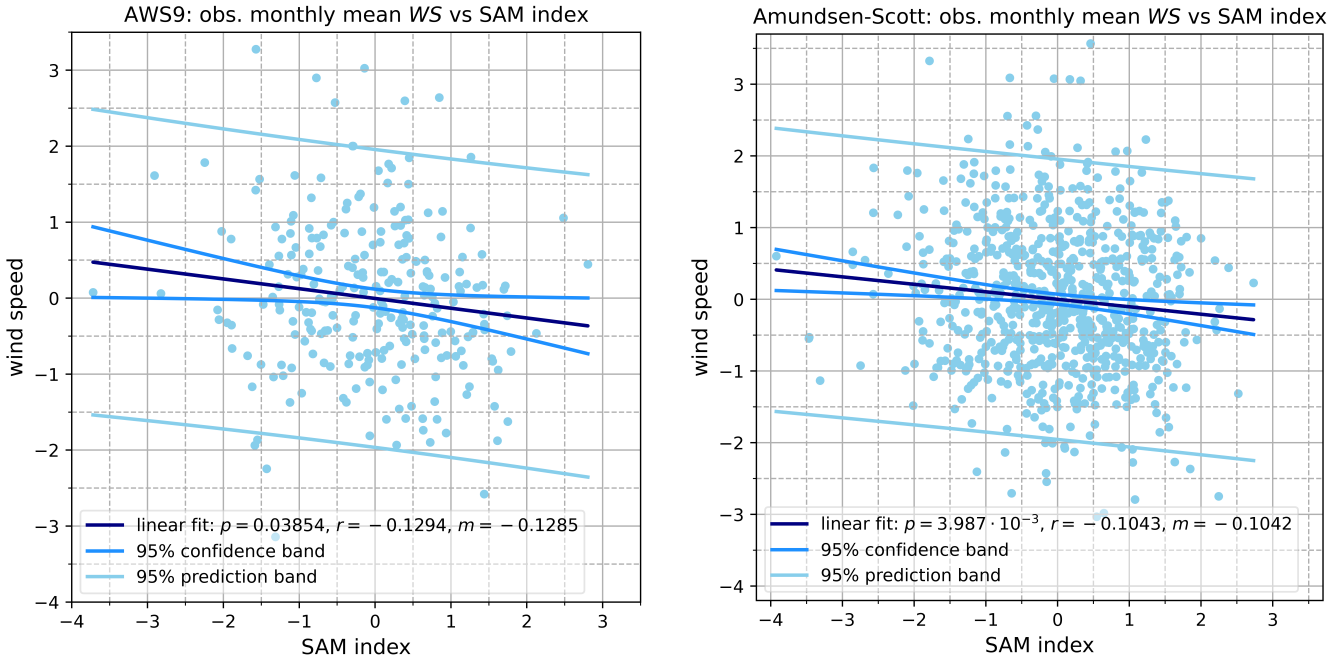

(a) (b)

Figure 22: Monthly mean wind speed versus the SAM index with linear regressions at **(a):** AWS9 (1998 Jan. to 2020 Sep.); **(b):** Amundsen-Scott Station (1957 Jan. to 2020 Dec.).

Because a positive SAM is expected to result both in less snow drift, due to lower wind speeds (found at AWS9 in section 4.2.2), and in less snowfall due to a reduction in advection of moisture to the Antarctic inland (Medley and Thomas, 2019)[23], the overall effect on monthly net snow accumulation on the Plateau is expected to be complicated or difficult to discern, and it is unclear whether an overall increase or decrease should be expected. The linear regression at AWS9 has $p = 0.01063$, $r = 0.1561$, and a slope of 0.1564, suggesting the overall effect to be a net increase with positive SAM. A scatter plot of the data at this site versus the SAM is shown in Figure 23.

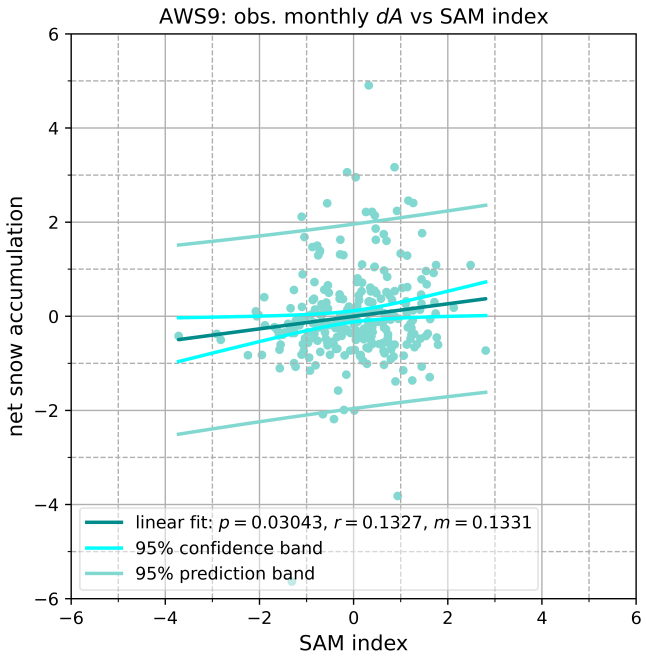

Figure 23: Monthly net snow accumulation versus the SAM index with linear regression, at AWS9.

Table 8: p-values, r-values, and slopes (m) of linear regressions versus SAM with $p < 0.05$.

Station	θ vs SAM	T vs SAM	WS vs SAM	dA vs SAM
AWS8	$p > 0.05$	$p > 0.05$	$p > 0.05$	$p > 0.05$
AWS9	$p = 0.03070$ $r = -0.1311$ $m = -0.1308$	$p = 1.754 \cdot 10^{-4}$ $r = -0.2256$ $m = -0.2252$	$p = 0.03854$ $r = -0.1294$ $m = -0.1285$	$p = 0.01063$ $r = 0.1327$ $m = 0.1331$
AWS12	$p = 2.641 \cdot 10^{-4}$ $r = -0.3607$ $m = -0.3607$	$p = 6.494 \cdot 10^{-6}$ $r = -0.4379$ $m = -0.4379$	$p > 0.05$	$p > 0.05$
AWS13	$p = 5.599 \cdot 10^{-5}$ $r = -0.3954$ $m = -0.3954$	$p = 1.113 \cdot 10^{-6}$ $r = -0.4690$ $m = -0.4690$	$p > 0.05$	$p > 0.05$
Amundsen-Scott	$p = 2.893 \cdot 10^{-12}$ $r = -0.2487$ $m = -0.2484$	$p = 1.034 \cdot 10^{-24}$ $r = -0.3588$ $m = -0.3585$	$p = 3.987 \cdot 10^{-3}$ $r = -0.1043$ $m = -0.1042$	$p > 0.05$
Vostok	$p = 6.078 \cdot 10^{-22}$ $r = -0.3521$ $m = -.03521$	$p = 5.710 \cdot 10^{-38}$ $r = -0.4593$ $m = -0.4593$	$p > 0.05$	$p > 0.05$

SO index

For the SOI, linear regressions with $p < 0.05$ were not found for any of the observational meteorological variables at any of the stations, suggesting that the influence of the SOI might not reach far enough inland to affect these Plateau sites. For (potential) temperature in particular, this is contrary to the expectation that a negative SOI would be associated with lower (potential) temperatures and a positive SOI with higher. For (potential) temperature and wind speed, the fits closest to significance are found at the lower-elevation stations (Amundsen-Scott Station and AWS8, respectively), suggesting that any effect of the SO that is present is stronger at lower elevations and closer to the coasts. The influence of the SO on Antarctica has been found previously primarily in West Antarctica and the Antarctic peninsula (e.g. Welhouse et al., 2016)[38]; of the stations used in this study, AWS8 and Aumundsen-Scott Station are indeed among those located nearest these regions.

5.3.2 EOF analysis

Because for most locations the correlations between both wind speed and net snow accumulation with the SAM and SOI were statistically insignificant, and because the EOFs are calculated from the correlation coefficients, any interpretation of these EOFs is likely to lead to dubious conclusions. Indeed, EOF analyses for these variables were found to reveal no clear relationships. Therefore, EOF analysis for wind speed and net snow accumulation will not be discussed. Temperature and potential temperature have mostly statistically significant correlations with the SAM, but no statistically significant correlations with the SOI, suggesting that these EOF analyses might also result in questionable conclusions. However, especially with regard to findings related to the SAM in particular, these analyses are more likely to be worthy of examination, and will be discussed here.

For temperature and potential temperature at each station and the SAM and SOI, the resulting EOF vectors have first, second, and third elements corresponding to (potential) temperature, SAM, and SOI, respectively. The EOFs and the percent of variance represented by each are presented in Table 9.

For both temperature and potential temperature at all stations, the EOF that corresponds to the largest proportion of the variance (about 38-49%) was found to be that which represents a negative association with both SAM and SOI, with a strong coupling between (potential) temperature and SAM, and a weaker SOI component. For the AWS data, the second EOF is dominated by the SOI, and represents a positive association between (potential) temperature and SOI, with a weak negative SAM component. For data from Amundsen-Scott and Vostok Stations, the second EOF differs only in the weak SAM component being positive rather than negative. The third EOF at all stations represents a positive association between (potential) temperature and SAM, with a weaker negative SOI component.

For the SAM, these results are consistent with the previous findings that the positive SAM phase is linked to lower temperature on the Plateau, and that the influence of the SAM is stronger than that of the SO in this region (Fogt and Marshall, 2020; Jones et al., 2019; Kwok and Comiso, 2002; van den Broeke and van Lipzig, 2004)[9][14][15][36]. The negative association is represented in the first EOF at all stations, and the first EOFs also indicate that this linkage explains more of the variance in (potential) temperature than the the effects of the SO. They also indicate a relation

between positive SOI and cooling in East Antarctica, and that this influence is weaker than that of the SAM, which is also consistent with the results of prior investigations (Welhouse et al., 2016)[38].

Table 9: The first, second, and third EOFs for (potential) temperature, SAM, and SOI at each station, with the percent of the variance represented by each EOF given with each vector.

Station	EOF	Potential temperature	Temperature
AWS8	1	38.557%, $(0.6344, -0.6286, -0.4499)$	41.265%, $(0.6775, -0.6870, -0.2628)$
	2	32.010%, $(0.2980, -0.3381, 0.8927)$	32.767%, $(0.2251, -0.1466, 0.9632)$
	3	29.433%, $(0.7133, 0.7003, -0.02718)$	25.9679%, $(0.7003, 0.7117, -0.05535)$
AWS9	1	38.425%, $(0.6176, -0.6994, -0.3597)$	41.342%, $(0.6702, -0.7017, -0.2417)$
	2	33.125%, $(0.4803, -0.02674, 0.8767)$	33.116%, $(0.3027, -0.03885, 0.9523)$
	3	28.450%, $(0.6228, 0.7142, -0.3194)$	25.542%, $(0.6776, 0.7114, -0.1864)$
AWS12	1	46.456%, $(0.6592, -0.6978, -0.2804)$	48.974%, $(0.6714, -0.6972, -0.2511)$
	2	32.735%, $(0.3402, -0.05580, 0.9387)$	32.626%, $(0.2843, -0.07063, 0.9561)$
	3	20.810%, $(0.6706, 0.7141, -0.2006)$	18.401%, $(0.6844, 0.7134, -0.1508)$
AWS13	1	47.237%, $(0.6706, -0.7068, -0.2253)$	49.685%, $(0.6789, -0.7045, -0.2068)$
	2	33.308%, $(0.3162, -2.390 \cdot 10^{-3}, 0.9487)$	33.113%, $(0.2702, -0.02221, 0.9626)$
	3	19.454%, $(0.6711, 0.7074, -0.2219)$	17.201%, $(0.6828, 0.7093, -0.1753)$
Amundsen-Scott	1	41.699%, $(0.6929, -0.7145, -0.0966)$	45.363%, $(0.6992, -0.7107, -0.07756)$
	2	34.030%, $(0.2669, 0.1297, 0.9550)$	33.763%, $(0.1941, 0.08429, 0.9774)$
	3	24.271%, $(0.6698, 0.6875, -0.2806)$	20.874%, $(0.6880, 0.6985, -0.1969)$
Vostok	1	45.208%, $(0.6968, -0.7091, -0.1081)$	48.775%, $(0.7003, -0.7078, -0.09291)$
	2	33.495%, $(0.1871, 0.03424, 0.9817)$	33.396%, $(0.1449, 0.01349, 0.9894)$
	3	21.299%, $(0.6924, 0.7043, -0.1566)$	17.829%, $(0.6990, 0.7063, -0.1120)$

6 Investigation of ERA5 data

This section presents findings for the ERA5 data at the approximate coordinates of AWS 8, 9, 12, and 13, Amundsen-Scott Station, and Vostok Station (introduced in section 2.2.1), and the ERA5-derived SAM and SO indices (section 3.3). As with the observational data (section 5), this section will examine Plateau climatology (section 6.1), trends with respect to time (6.2), and the influence of the indices (6.3). Because ERA5 gives longer records for the AWS sites than the observational data could provide, the calculations of climtological averages are more sound, more trends with respect to time are detected, more and stronger correlations with the SAM and SO indices are found, and the EOF analyses are stronger. All of these findings will be discussed in the context of the results for observational data (section 5).

6.1 Plateau climatology

As expected, the 2m (potential) temperature climatologies follow similar patterns at all locations, and are nearly identical to the climatologies for observed (potential) temperatures, with the same prominent seasonal cycles and nearly the same amplitudes. The large changes in mean temperature during the transition periods between summer and winter are slightly smaller – typically around ±5 to 10°C per month – and follow the same pattern with respect to elevation.

These findings show the same general spatial pattern as the observational temperatures. However, the ERA5 2m (potential) temperature climatologies were found to indicate slightly warmer winters and slightly colder summers than the observational data showed. While the maximum average monthly potential temperature is within ±5°C of 0°C at all locations, the minima vary by location. At AWS 8 and 9, the minima are approximately −18 to −20°C, while farther inland, the remaining four stations have minima of approximately −27 to −30°C. This demonstrates that ERA5 is reproducing the the more extreme cold winters farther inland, even adjusting for elevation. In terms of actual temperature, AWS8 is found to be the warmest site (Figure 24a), followed by AWS9. AWS12 (Figure 24b), AWS13, and Vostok Station all have similar ranges of average monthly temperature, from about −34°C to about −61°C.

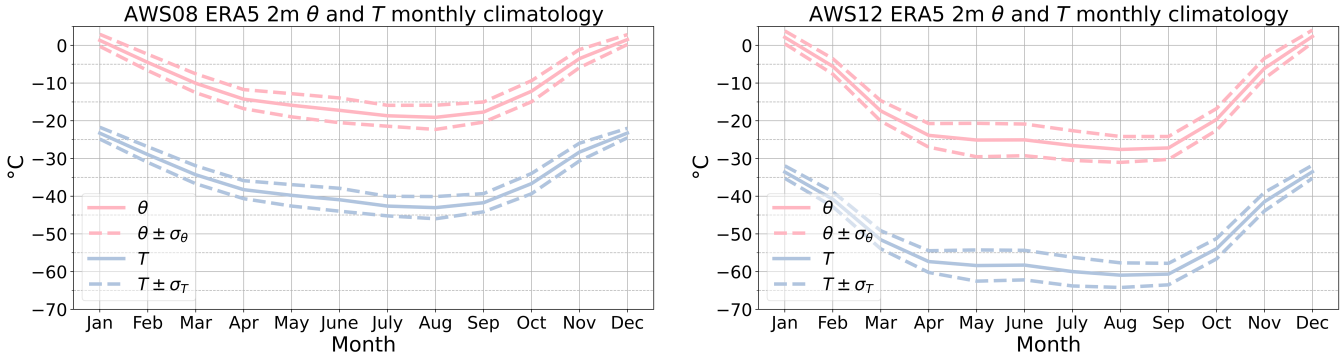

(a) (b)

Figure 24: Selected examples of monthly mean 2m (potential) temperature climatologies for ERA5 data (1981 Jan. to 2020 Dec.), with their respective standard deviation bands, at **(a):** AWS8; **(b):** AWS12.

As with the findings for observational data, comparing 2m potential temperature time series between locations using scatter plots and linear regressions shows clear indications of the spatial pattern and seasonal cycle. The latter results in strong correlations for every pair of sites and scatter plots with distinct clusters for the summer, winter, and transitionary months. Values during the summer remain very similar at all locations, and AWS 8 and 9 again have quite similar values throughout the year. Winter values still tend to be lower farther inland and at higher elevation. However, unlike for the observational time series, the ERA5 2m potential temperature at AWS13 and Vostok Station tend to be quite similar in winter, rather than AWS 12 and 13 having very similar values and Vostok Station having the clear lowest; scatter plots illustrating this are shown in Figure 25.

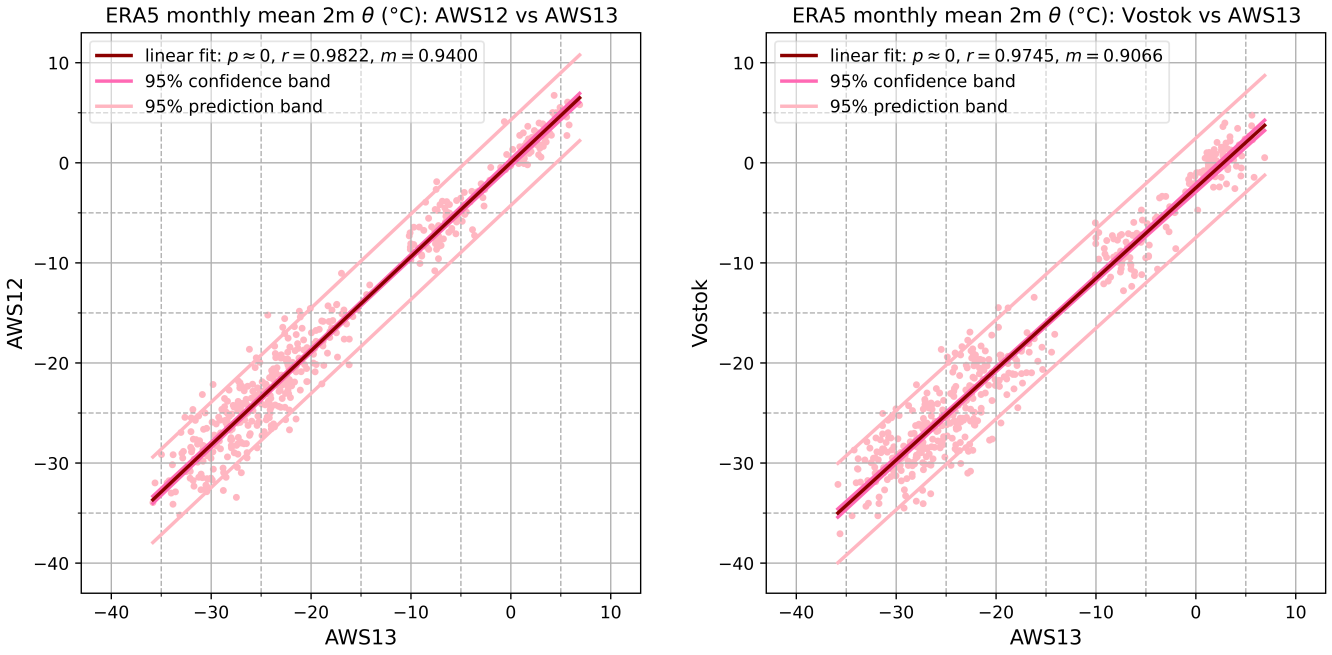

(a) (b)

Figure 25: Scatter plots with linear regressions comparing ERA5 monthly mean 2m potential temperature time series (1981 Jan. to 2020 Dec.) at **(a):** AWS 12 and 13; **(b):** AWS13 and Vostok Station.

As seen with observed wind speeds, the 10m wind speed climatologies each follow a pattern of higher speeds during colder times of year and lower speeds during the warmer months, demonstrating the importance of low surface temperature in driving the katabatic wind. The lowest average wind speeds are consistently found in December or January, the same months as the minima for observed wind speeds. The highest average 10m wind speeds are found in June and July, far more consistent than the observational findings, for which no two sites had their maxima in the same month. AWS 9, 12, and 13 also each have a local minimum in either September or October, which is followed in each case by a local maximum the next month. Additionally, AWS12 has a local maximum in February, followed by a local minimum in March. In Figure 26a, the 10m wind speed climatology at AWS8 is shown as an example of the typical pattern, while the climatology at AWS12

is provided in 26b as an example of the additional local extrema seen at some sites. In the observational data, such a relatively smooth curve was found only at Amundsen-Scott Station.

Maximum wind speeds have a noteworthy difference in magnitude at the lower-elevation locations (AWS 8 and 9, and Amundsen-Scott Station) compared to the higher-elevation locations (AWS 12 and 13, and Vostok Station), a pattern that was not evident in the observational wind speed climatologies; this difference is illustrated in Figure 26, using AWS 8 and 12 as examples. The highest average wind speed among the higher-elevation locations is 4.876 m s^{-1} at Vostok Station in June, while the highest among the lower-elevation locations is 5.953 m s^{-1} at Amundsen-Scott Station in July. The higher-elevation sites represent locations on the upper Plateau, where local surface slopes are relatively small and where the atmospheric boundary layer tends to be more stable, especially in winter. Meanwhile the lower-elevation sites are within the katabatic zone, where higher average wind speeds are expected due to the surface slope and the temperature inversion present at higher elevations.

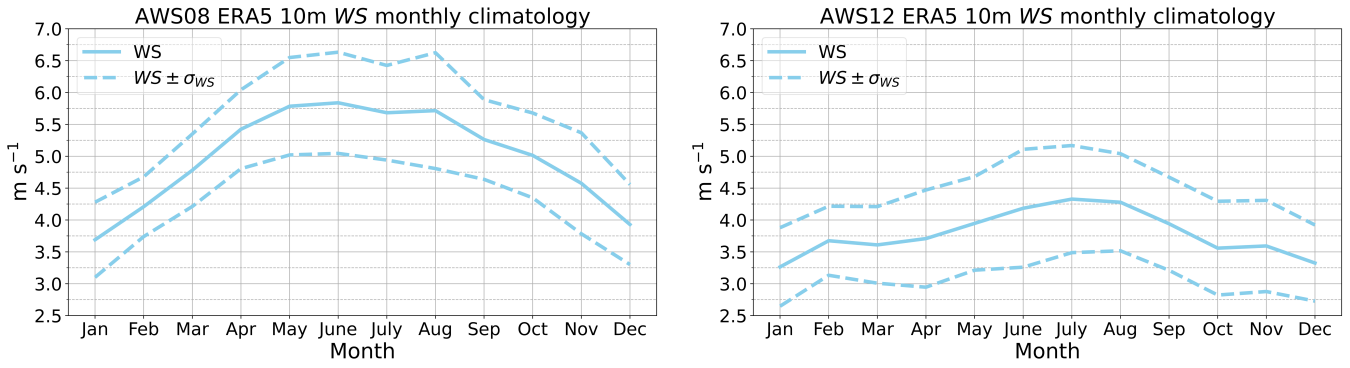

(a) (b)

Figure 26: Selected examples of monthly mean 10m wind speed climatologies for ERA5 data (1981 Jan. to 2020 Dec.), with their respective standard deviation bands, at **(a):** AWS8; **(b):** AWS12.

Similarly to the findings for observational wind speed data, the scatter plots and linear regressions comparing ERA5 10m wind speed between sites are of limited usefulness. Although all combinations have linear regressions with $p < 0.05$ and the correlations are slightly improved, for most pairs the correlations remain weak. Of the fifteen combinations, only four pairs had $r > 0.5$: the pair of AWS 12 and 13, and the three combinations of AWS 8 and 9 and Amundsen-Scott Station. This is indicative of the similar elevations and surface slopes at Amundsen-Scott Station and AWS8/9 resulting in somewhat similar wind speeds, in addition to the importance of proximity. The scatter plot for AWS8 and Amundsen-Scott Station is shown in Figure 27a, along with an example of a more typical comparison with weak correlation in Figure 27b.

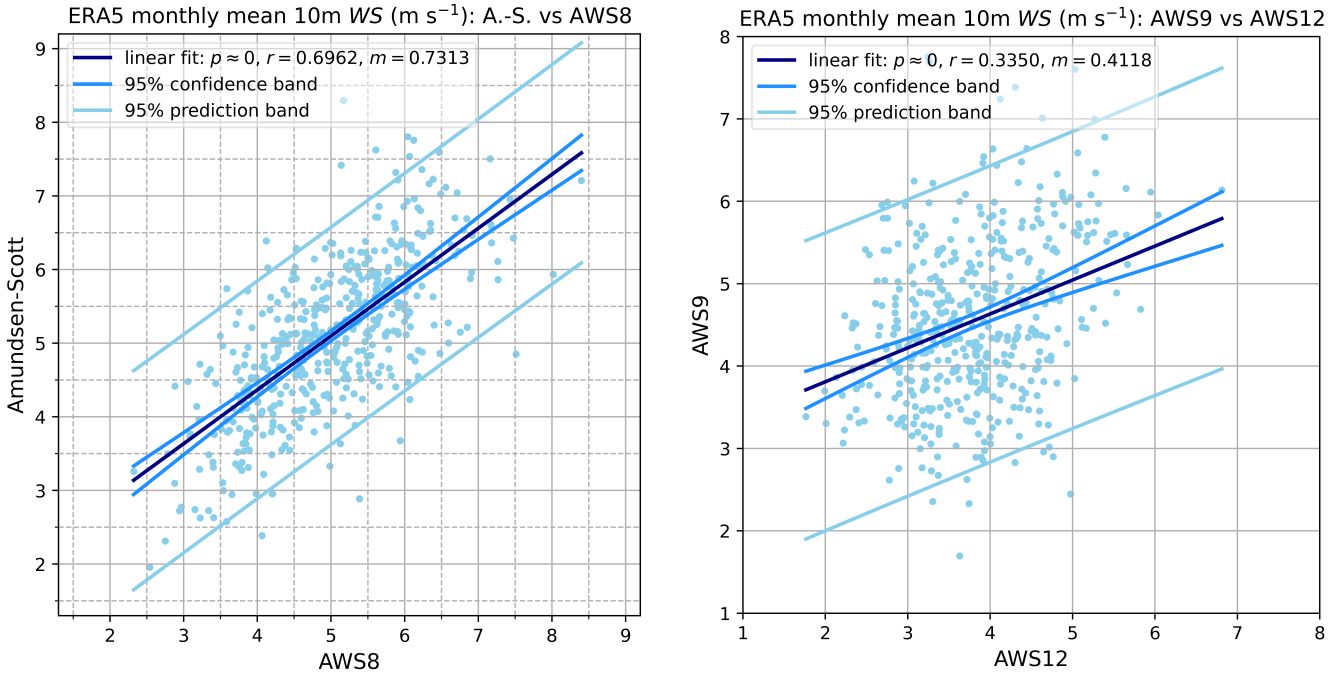

(a) (b)

Figure 27: Scatter plots with linear regressions comparing ERA5 monthly mean 10m wind speed time series (1981 Jan. to 2020 Dec.) at **(a):** AWS8 and Amundsen-Scott Station; **(b):** AWS 9 and 12.

A notable feature of the ERA5 snowfall climatologies is that the values found in peak snowfall months are approximately two orders of magnitude smaller than the peaks in the observational monthly net snow accumulation climatologies. It is unclear why this should be the case; it might be reasonable to expect that the opposite would occur, since net accumulation also includes removal processes. The fact that ERA5 snowfall values are an average over each grid box does mean that comparisons with data from specific sites is imperfect, but because this discrepancy occurs at all of the four stations for which snow accumulation data are available, this could be an indication that the ERA5 reanalysis might have difficulty accurately simulating snowfall on the Plateau. In particular, the difficulty might lie in reproducing the highly episodic nature of precipitation on the Plateau.

Similarly to the observed monthly net snow accumulation, the climatologies for monthly total snowfall have large monthly standard deviations and do not closely follow a general pattern, but some similar features are present. At all locations, reduced snowfall occurs during the colder months of the year, with all sites experiencing at least one local minimum in the range of July to October. With the exception of AWS13, every location also has a local minimum in average monthly snowfall in December, January, or February. Whether the absolute minimum occurs in the winter months or in summer does not follow a pattern with respect to either elevation or proximity; despite Vostok Station being nearest to AWS 12 and 13 and sharing a similar elevation, its monthly snowfall climatology more closely resembles that of Amundsen-Scott Station. This could be related to the distance inland, such that Amundsen-Scott and Vostok Stations receive more moisture advected inland, compared to AWS 12 and 13 near and at the southern pole of inaccessibility.

A more consistent commonality between the monthly snowfall climatologies is found in their maxima. All sites except AWS13 have local maxima in either October or November, as temperatures are rising following the coldest part of the year, and as the weakening meridional temperature and pressure gradients result in weaker circumpolar currents and more exchange of air masses with lower latitudes, so that more moisture is carried to the Plateau from lower latitudes. However, the largest amounts of snowfall at every location occur during February to May, as temperatures are falling after the brief Antarctic summer and the air is able to hold less moisture. All sites have at least a local maximum in average monthly snowfall in either April or May, and for all except AWS 12 and 13, this is the absolute maximum; AWS 12 and 13 have their absolute maxima in February.

Even more so than for wind speed, elevation and distance from the coast have a noteworthy relation to average monthly snowfall. As illustrated by the examples at AWS 8 and 12 in Figure 28, at the lower-elevation locations (AWS 8 and 9, and Amundsen-Scott Station) both the maximum and minimum values of average monthly snowfall tend to be larger than the values at the higher-elevation locations (AWS 12 and 13, and Vostok Station) by a factor of about 2-3. In the case of Vostok Station, the maximum (0.05290 mm w.e.) is considerably lower than the maxima at AWS 12 or 13, so that the maxima at the lower-elevation stations are nearly five times larger than that of Vostok Station. This can be attributed in part to the smaller amounts of moisture that are advected farther inland, and in part to the more extreme cold of the upper Plateau reducing the moisture capacity of the atmosphere so that very little water is available to precipitate.

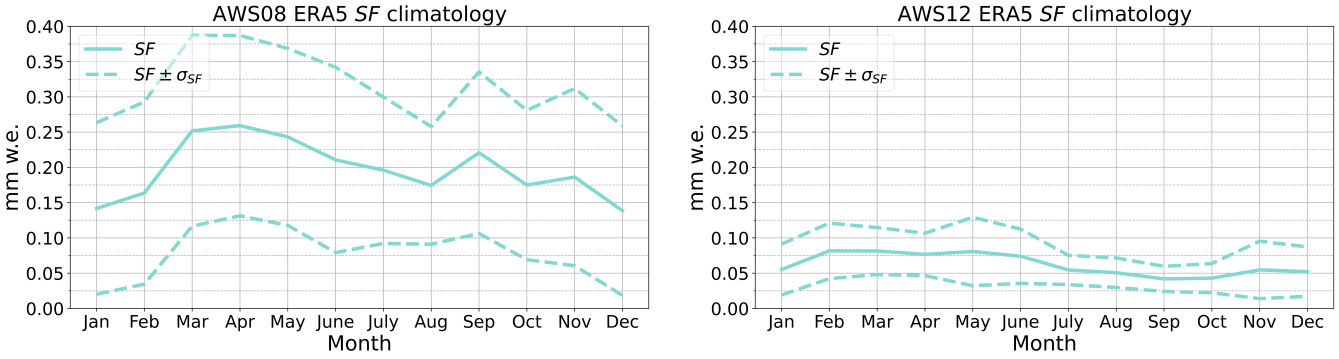

(a) (b)

Figure 28: Selected examples of monthly total snowfall climatologies for ERA5 data (1981 Jan. to 2020 Dec.), with their respective standard deviation bands, at **(a):** AWS8; **(b):** AWS12.

While comparisons between locations for ERA5 monthly snowfall found correlations with $p < 0.05$ for eight of fifteen pairs (compared to one of four for observed monthly net snow accumulation), most of these correlations were still weak, with only two found to have $r > 0.5$: AWS 8 and 9 (shown as an example in Figure 29), and AWS 12 and 13. These pairs were anticipated to likely be more correlated than most others, due to proximity and similar elevations and surface slopes. It is noteworthy that for Vostok Station only one significant (and weak, $r = 0.2611$) correlation was found, with Amundsen-Scott Station, likely due to the unique surface topography of Vostok Station. Some other results of these comparisons are difficult to interpret. Snowfall at AWS8 was found to be more strongly correlated with that of AWS12 than with Amundsen-Scott Station (illustrated in Figure 29b and 29d), despite the opposite being expected. Additionally, both AWS 12 and 13

were found to have stronger correlations with AWS9 than with AWS8 (example of AWS12 shown in Figure 29c and 29d), a difference not explained by proximity or similar elevation, which occurs despite the expectation that snowfall at AWS 8 and 9 would be quite similar.

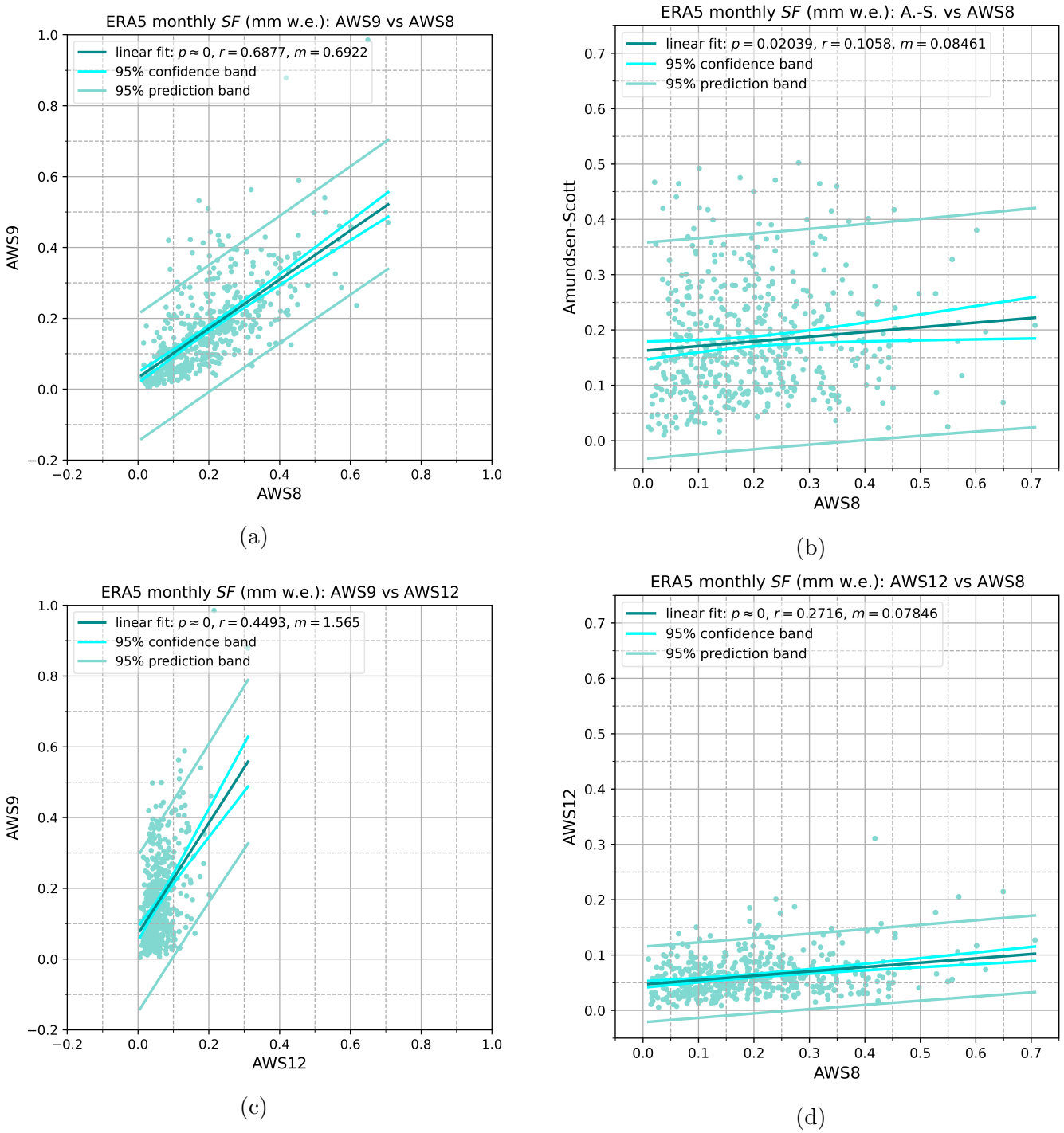

Figure 29: Scatter plot with linear regression comparing ERA5 monthly snowfall time series (1981 Jan. to 2020 Dec.) at **(a):** AWS 8 and 9; **(b):** AWS8 and Amundsen-Scott Station; **(c):** AWS 9 and 12; **(d):** AWS 8 and 12.

6.2 Monthly mean time series, and linear trends

The monthly mean time series for 2m (potential) temperature at every location are very similar to those of observations and follow the pattern of the climatologies rather closely. As with the observed (potential) temperatures, linear least-squares regressions detected no trends with respect to time with $p < 0.05$ for either temperature or potential temperature at any location. The time series for monthly mean (potential) temperature at Vostok Station are shown in Figure 30 as examples.

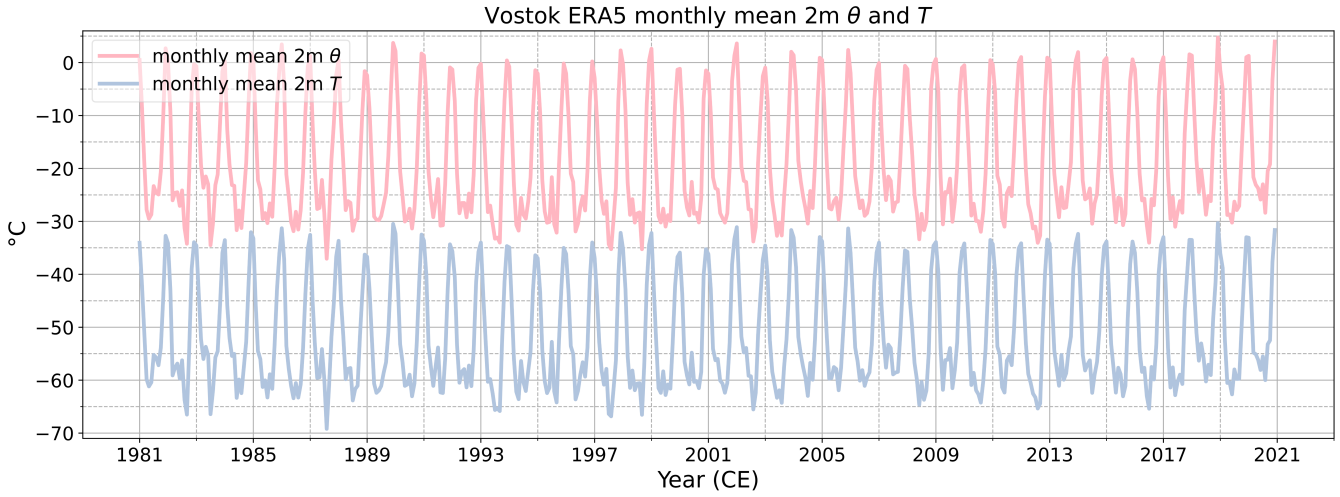

Figure 30: Time series for monthly mean 2m (potential) temperature at Vostok Station, from ERA5 data for 1981 Jan. to 2020 Dec.

Monthly mean 10m wind speeds exhibit noticeably more variability than (potential) temperature, so it is difficult to visually identify a yearly cycle in the time series. For most years, each time series has one or two clearly visible peaks, but both larger numbers and zero per year also occur fairly frequently. Linear least-squares regressions detected $p < 0.05$ trends in monthly mean 10m wind speed with respect to time at all locations except for AWS8. These trends all have weak positive correlations ($r = 0.1394$, at most), opposite the findings for observational wind speeds (section 5.2). This difference could be related to the measurement height – since observations of wind speed are measured at approximately 4.72m at the highest, these findings could suggest that 10m wind speed is experiencing differing trends from wind speeds at lower heights. Another possibility for the AWS sites is simply that the longer time series provided by ERA5 could be allowing for detection of longer-term trends that differ from the shorter-term trends found in the observational time series. The strongest trend was found at AWS9, with a slope of $m = 0.1066$ m s^{-1} per decade ($p = 5.289 \cdot 10^{-3}$), and the weakest at AWS13, with a slope of $m = 0.07231$ m s^{-1} per decade ($p = 0.02926$). The wind speed time series for Vostok Station is shown together with its trend line in Figure 31, and a summary of the p-values, r-values, and slopes of the $p < 0.05$ linear regressions is presented in Table 10.

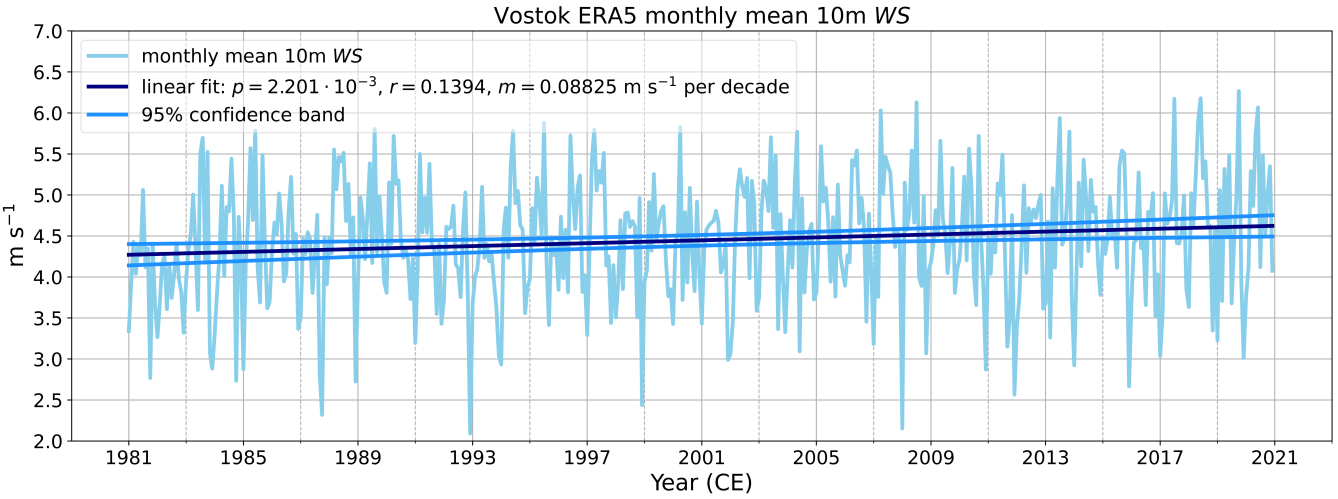

Figure 31: Time series for monthly mean 10m wind speed at Vostok Station, from ERA5 data for 1981 Jan. to 2020 Dec.

Table 10: p-values, r-values, and slopes (m) of linear regressions for monthly mean 10m wind speed versus time, shown for those with $p < 0.05$.

Station	Wind speed vs time
AWS9	$p = 5.289 \cdot 10^{-3}$ $r = 0.1271$ $m = 0.1066$ m s^{-1} per decade
AWS12	$p = 9.972 \cdot 10^{-3}$ $r = 0.1175$ $m = 0.08019$ m s^{-1} per decade
AWS13	$p = 0.02926$ $r = 0.09951$ $m = 0.07231$ m s^{-1} per decade
Amundsen-Scott	$p = 0.01337$ $r = 0.1128$ $m = 0.1020$ m s^{-1} per decade
Vostok	$p = 2.201 \cdot 10^{-3}$ $r = 0.1394$ $m = 0.08825$ m s^{-1} per decade

The monthly total snowfall time series, while also showing more variability than (potential) temperature, display fairly recognizable yearly patterns similar to the climatologies. The time series at all locations display large peaks in snowfall during the first half of the year, and typically smaller peaks later in the year. All locations experience irregular years of noticeably larger than usual amounts of snowfall, which may be related to the SAM and SO cycles (investigated in section 6.3). Linear least-squares regressions detected no $p < 0.05$ trends with respect to time at any location. The time series for monthly total snowfall at Vostok Station is shown in Figure 32 as an

example.

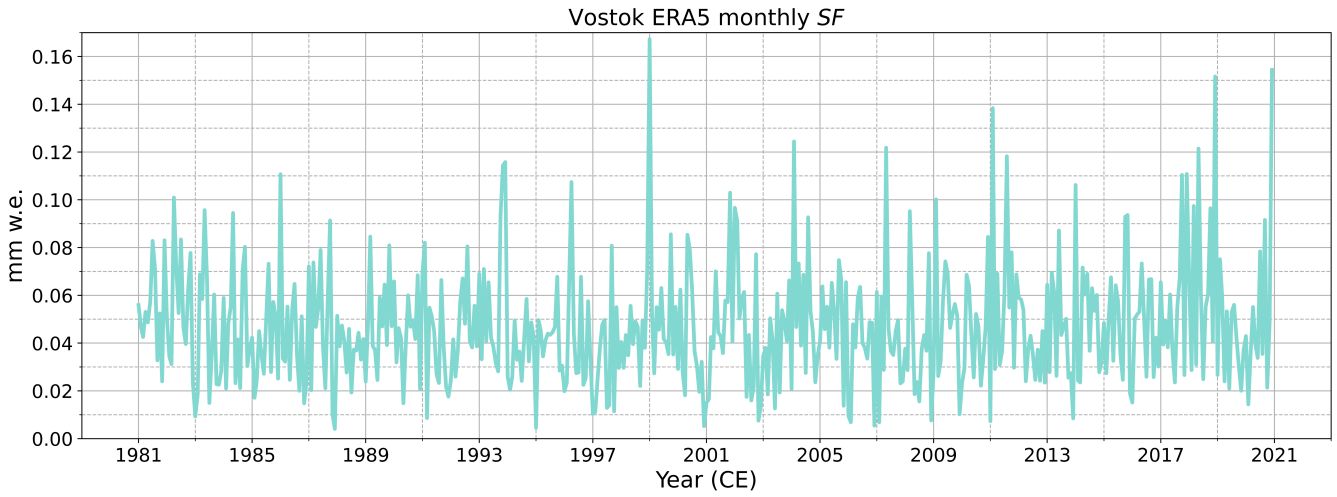

Figure 32: Time series for monthly total snowfall at Vostok Station, from ERA5 data for 1981 Jan. to 2020 Dec.

6.3 Influences of the SAM and SO indices

After each times series for ERA5 (potential) temperature, wind speed, snowfall, ERA5-derived SAM and SO indices had been detrended, deseasonalized, and standardized (section 3.6), then associations between the meteorological variables and these indices were investigated, first using linear least-squares regressions, and then with empirical orthogonal function (EOF) analysis.

6.3.1 Linear regressions versus the indices

SAM index

For the SAM, linear regressions with $p < 0.05$ were found for 2m potential temperature at all locations except AWS8 and 2m temperature at all locations. For 10m wind speed, $p < 0.05$ linear regressions were found at all locations except Vostok Station, and for snowfall only at AWS 8 and 13. This suggests that the SAM has a detectable effect on (potential) temperatures and wind speeds over much of the Plateau, while its influence on snowfall appears to be more limited. A summary of the p-values, r-values, and slopes of the $p < 0.05$ fits is presented in Table 11.

As with the observed (potential) temperatures, of the locations with $p < 0.05$ fits for ERA5 2m (potential) temperature, these correlations are all negative, and the strength of the correlations generally increases for locations farther inland, where conditions are likely more more sensitive to the effects of the SAM. The weakest correlation for potential temperature is found at AWS9 ($r = -0.1117$), and the weakest for temperature is found at AWS8 ($r = -0.1338$), while the strongest correlations are found at AWS13 ($r = -0.3650$ for potential temperature and $r = -0.4477$ for temperature). Correlations at all locations are stronger for temperature than for potential temperature, possibly indicating a weaker influence of the SAM on the surface pressure than on the temperature near the surface.

Compared with the findings for observational time series, the ERA5 2m (potential) temperatures and SAM index were found to be more significantly correlated at the AWS sites and less so at Amundsen-Scott and Vostok Stations, due to the AWS records being shorter than the ERA5 time series and the records from the READER archive being longer. This resulted in the detection of an additional significant correlation, for temperature versus SAM at AWS8, so that the total number of significant ERA5 2m (potential) temperature correlations versus the SAM is eleven of twelve, compared to ten of twelve for the observational data. However, the correlations for the ERA5 data were also found to be weaker, regardless of location or degree of significance, suggesting that ERA5 might not fully represent the effect of the SAM on the (potential) temperature of the Plateau.

Scatter plots of the AWS13 (potential) temperature versus SAM are shown as examples in Figure 33.

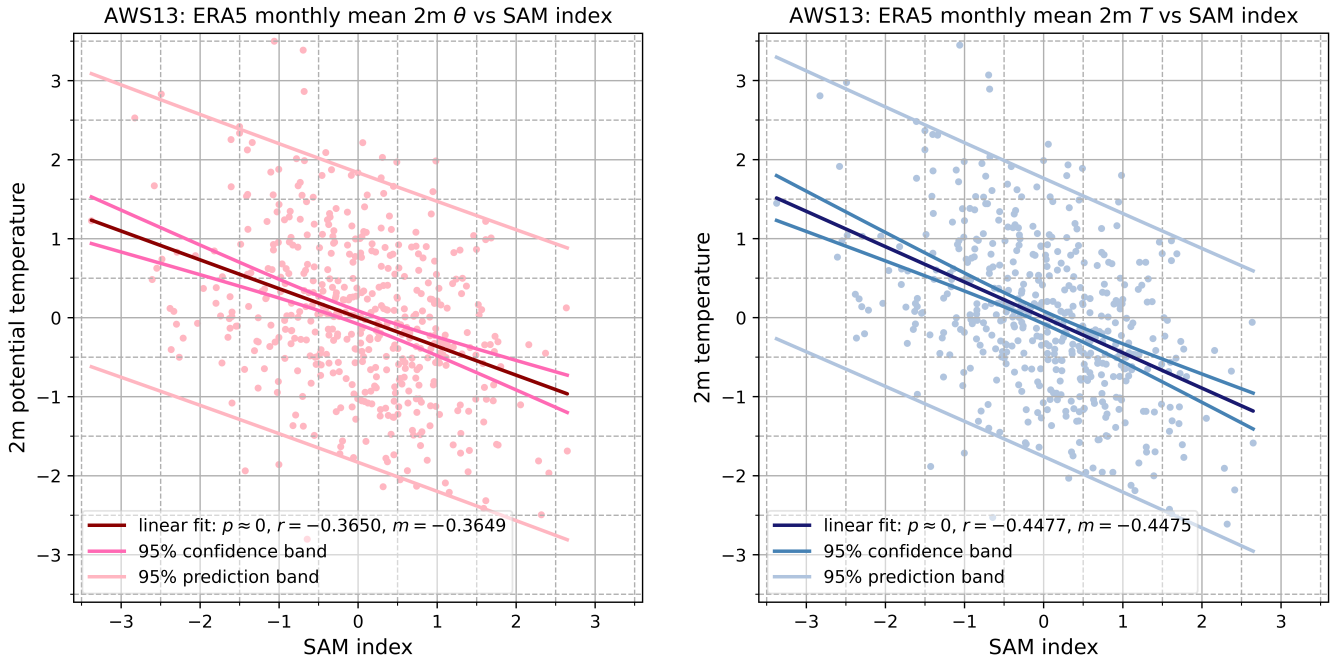

(a) (b)

Figure 33: ERA5 monthly mean **(a):** 2m potential temperature; **(b):** 2m temperature versus the SAM index with linear regressions, at AWS13.

Of the locations with $p < 0.05$ 10m wind speed fits versus the SAM, there was no clear connection between correlation strength and either elevation or distance inland. All of these correlations were found to be negative, which is consistent with expectation that a positive SAM phase results in lower wind speeds near the surface due to increasing the stability of the surface boundary layer (Schneider et al., 2012b; van den Broeke and van Lipzig, 2004)[29][36]. The weakest correlation is found at Amundsen-Scott Station (−0.1868), followed by AWS8 (−0.2041), and the strongest is found at AWS12 (−0.2800), followed by AWS9 (−0.2746). These findings are in agreement with the correlations found for observed wind speeds versus the SAM (section 5.3). A scatter plot for the AWS9 wind speed versus SAM is shown in Figure 34.

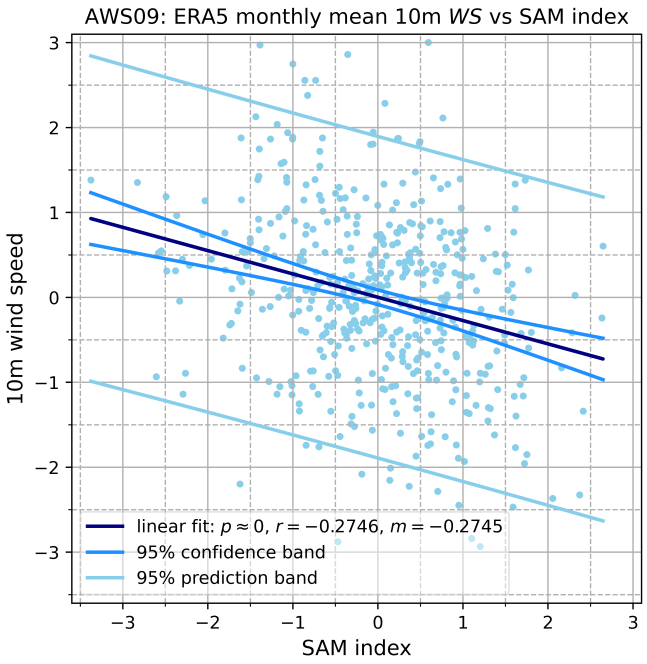

Figure 34: ERA5 monthly mean 10m wind speed at AWS9 versus the SAM index, with linear regression.

Despite the longer time series available for ERA5 snowfall, only two locations were found to have $p < 0.05$ linear regressions versus the SAM: a positive correlation at AWS8 ($r = 0.1755$) and a negative correlation at AWS13 ($r = -0.1189$). The positive correlation found for observed net monthly snow accumulation at AWS9 versus the observational SAM index did not correspond to a correlation between ERA5 snowfall at AWS9 versus the ERA5 SAM index. Although two statistically significant correlations were found for ERA5 data compared to only one for observational monthly net snow accumulation, the small number of significant correlations in both cases suggests that the influence of the SAM is either not present at all locations or is not consistently detectable in these datasets by these methods. Because a positive SAM is expected to correspond to less transport of moisture to the Antarctic inland (Medley and Thomas, 2019)[23], negative correlations were expected at Plateau locations. These findings, however, provide some possible evidence that a positive SAM corresponds to reduced snowfall farther inland and increased snowfall closer to the edges of the Plateau. Scatter plots of snowfall versus the SAM at AWS8 and AWS13 are shown in Figure 35.

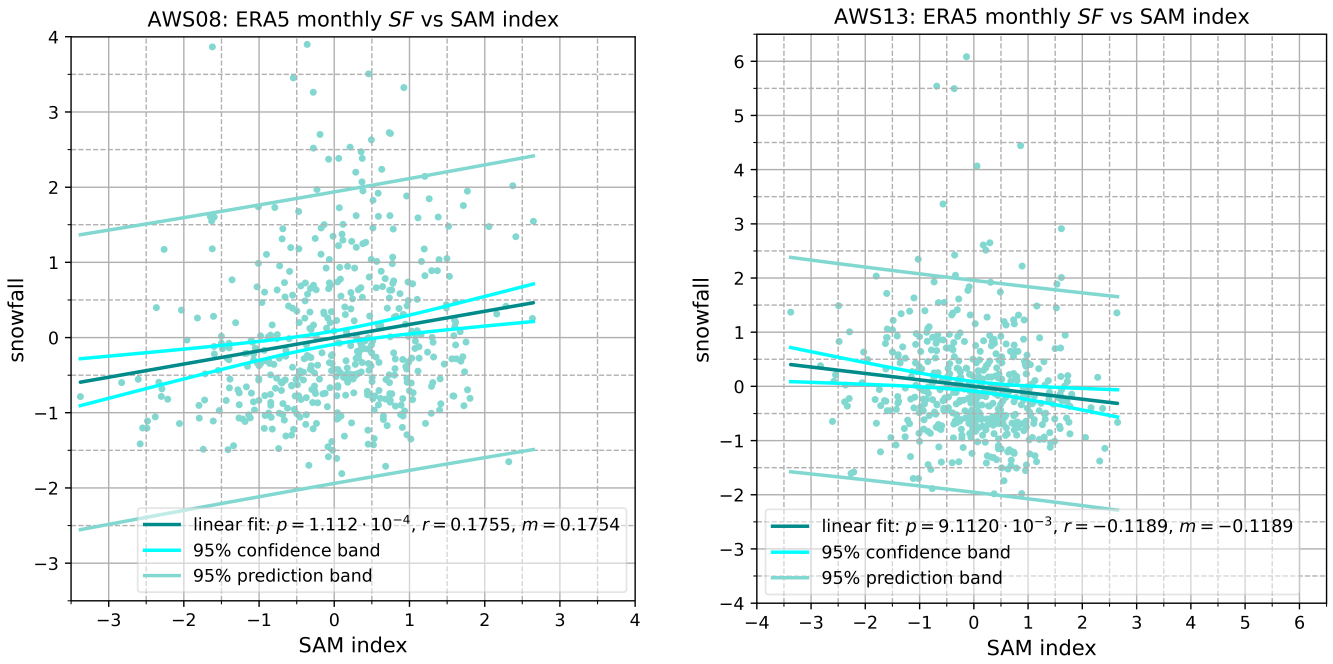

(a) (b)

Figure 35: ERA5 monthly snowfall at **(a):** AWS8; **(b):** AWS9 versus the SAM index, with linear regressions.

Table 11: p-values, r-values, and slopes (m) of linear regressions versus SAM with $p < 0.05$.

Station	θ vs SAM	T vs SAM	WS vs SAM	SF vs SAM
AWS8	$p > 0.05$	$p = 2.376 \cdot 10^{-3}$ $r = -0.1338$ $m = -0.1384$	$p = 6.552 \cdot 10^{-6}$ $r = -0.2041$ $m = -0.2041$	$p = 1.112 \cdot 10^{-4}$ $r = 0.1755$ $m = 0.1754$
AWS9	$p = 0.01438$ $r = -0.1117$ $m = -0.1116$	$p = 4.227 \cdot 10^{-6}$ $r = -0.2082$ $m = -0.2081$	$p = 9.493 \cdot 10^{-10}$ $r = -0.2746$ $m = -0.2745$	$p > 0.05$
AWS12	$p = 4.220 \cdot 10^{-11}$ $r = -0.2951$ $m = -0.2950$	$p = 2.677 \cdot 10^{-18}$ $r = -0.3839$ $m = -0.3837$	$p = 4.285 \cdot 10^{-10}$ $r = -0.2800$ $m = -0.2799$	$p > 0.05$
AWS13	$p = 1.436 \cdot 10^{-16}$ $r = -0.3650$ $m = -0.3649$	$p = 4.939 \cdot 10^{-25}$ $r = -0.4477$ $m = -0.4475$	$p = 7.402 \cdot 10^{-8}$ $r = -0.2426$ $m = -0.2425$	$p = 9.112 \cdot 10^{-3}$ $r = -0.1189$ $m = -0.1189$
Amundsen-Scott	$p = 1.593 \cdot 10^{-4}$ $r = -0.1715$ $m = -0.1715$	$p = 7.816 \cdot 10^{-11}$ $r = -0.2911$ $m = -0.2911$	$p = 3.809 \cdot 10^{-5}$ $r = -0.1868$ $m = -0.1868$	$p > 0.05$
Vostok	$p = 9.531 \cdot 10^{-10}$ $r = -0.2748$ $m = -0.2747$	$p = 2.759 \cdot 10^{-19}$ $r = -0.3941$ $m = -0.3939$	$p > 0.05$	$p > 0.05$

SO index

For the SOI, linear regressions with $p < 0.05$ were found only for snowfall at AWS8 and Vostok Station, suggesting only a limited influence by the SO on the Plateau, similar to the findings for the observational data, for which no significant correlations with the SOI were found. The two statistically significant correlations found for snowfall are both positive, suggesting that a positive SO phase (La Niña episodes) corresponds with increased snowfall in at least some Plateau locations, which is consistent with the expectation that the positive SOI could correspond to increased advection of air masses from lower latitudes toward some regions of the Plateau. The correlation at AWS8, located farther from the Pacific coast of Antarctica, is weaker than the one at Vostok Staion. Although the scatter plots show a large amount of scattering even at these sites, the large number of data points was sufficient to find these weak significant correlations; the scatter plots with linear trends for snowfall versus SOI at AWS8 and Vostok Station are shown in Figure 36.

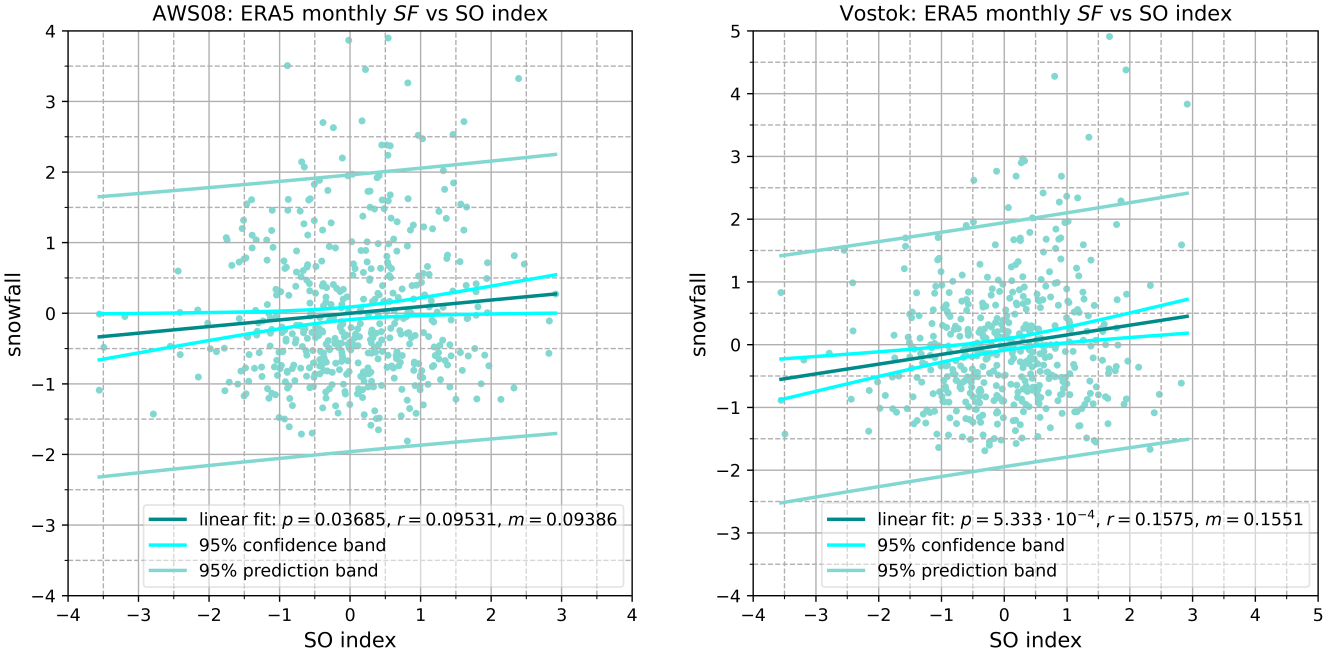

(a) (b)

Figure 36: ERA5 monthly snowfall at **(a):** AWS8; **(b):** Vostok Station versus the SOI, with linear regressions.

6.3.2 EOF analysis

Similarly to the cases of wind speed and net snow accumulation for the observational time series, because few statistically significant correlations were found for snowfall and either of the SAM and SO indices, EOF analysis for snowfall will not be examined. Additionally, as in the cases of (potential) temperature for the observational time series, the EOF analysis for ERA5 2m (potential) temperature and 10m wind speed are imperfect, but were considered worthy of discussion.

For the (potential) temperature-SAM-SOI system at each location, the resulting EOF vectors

have first, second, and third elements corresponding to (potential) temperature, SAM, and SOI, respectively. Similarly, the wind speed-SAM-SOI system results in EOF vectors with first components corresponding to wind speed. The EOFs and the percent of variance represented by each are presented for the (potential) temperature-SAM-SOI systems in Table 12 and the wind speed-SAM-SOI systems in Table 13.

For every variable and each location, the EOF that corresponds to the largest proportion of the variance (about 39-49%) was found to be that which indicates (potential) temperature or wind speed decreasing as SAM and SOI increase, while the SAM and SOI increase and decrease together. Comparing the first EOFs for temperature and potential temperature, at each location the temperature EOF has a larger temperature component and smaller SOI component. This suggests that the SO impacts potential temperature more than actual temperature, possibly because of the SO exerting a more direct influence on the surface pressure.

At locations farther inland and at higher elevation (AWS 12 and 13, and Vostok Station), the first EOFs for (potential) temperature are dominated by the SAM and (potential) temperature components, with weaker SOI components, while nearer the coast and at lower elevation (AWS 8 and 9, and Amundsen-Scott Station), the SAM and SOI components are closer to equal. This suggests that (potential) temperatures farther inland are impacted more by the SAM and less by the SOI. The first EOFs for wind speed do not have as clear a spatial pattern. While the first EOFs for wind speed at AWS12 and AWS13 are dominated by the SAM and wind speed components, the one for Vostok Station has the strongest SOI component among the first wind speed EOFs. This suggests that wind speeds are, in most cases, impacted more by the SAM and less by the SOI farther inland, except for Vostok Station, where wind speed is affected only weakly by either. Since the negative pressure anomalies the SAM represents occur directly over the Plateau, while those associated with the SO exist primarily off the coast of Antarctica, this is largely expected. Furthermore, the weak effect at Vostok Station can be understood as a result of the local surface topography, since it is located in a depression in the surface with a relatively small slope, allowing an unusually stable surface boundary layer to form in the vicinity, making it less susceptible to other forcings. These results are consistent with expectations that both positive SAM and positive SOI are linked to lower temperature and slower winds on the Plateau, and that the influence of the SAM is stronger than that of the SO in this region (Fogt and Marshall, 2020; Jones et al., 2019; Kwok and Comiso, 2002; van den Broeke and van Lipzig, 2004; Welhouse et al. 2016)[9][14][15][36][38].

For all three variables, almost all of the second EOFs are dominated by their first component and SOI component, both of which are positive, and have SAM components that are much smaller and vary in sign. The exception is again wind speed at Vostok Station, for which the second EOF suggests only a small influence from both indices. For the (potential) temperature second EOFs, the SOI component is larger and the (potential) temperature component smaller for the farther inland locations. Each third EOF represents the (potential) temperature or wind speed and the SAM increasing and decreasing together, with the SOI component doing the opposite. The third EOFs for (potential) temperature exhibit the same spatial pattern as the first EOFs with regard to distance inland and the relative weights of the (potential) temperature and SOI components.

Table 12: The first, second, and third EOFs for (potential) temperature, SAM, and SOI at each station, with the percent of the variance represented by each EOF given with each vector.

Station	EOF	Potential temperature	Temperature
AWS8	1	$38.822\%, (0.2013, -0.6975, -0.6878)$	$40.634\%, (0.4816, -0.6918, -0.5380)$
	2	$33.128\%, (0.9770, 0.09224, 0.1924)$	$32.735\%, (0.7523, 0.01139, 0.6588)$
	3	$28.050\%, (0.07075, 0.7107, -0.7000)$	$26.632\%, (0.4496, 0.7220, -0.5259)$
AWS9	1	$40.503\%, (0.4634, -0.6677, -0.5825)$	$42.788\%, (0.5698, -0.6772, -0.4656)$
	2	$31.986\%, (0.8232, 0.08098, 0.5620)$	$31.915\%, (0.5968, -0.04845, 0.8009)$
	3	$27.511\%, (0.3281, 0.7400, -0.5872)$	$25.298\%, (0.5649, 0.7342, -0.3765)$
AWS12	1	$44.851\%, (0.6204, -0.6954, -0.3627)$	$47.525\%, (0.6495, -0.6976, -0.3025)$
	2	$32.635\%, (0.4686, -0.04220, 0.8824)$	$32.658\%, (0.3773, -0.04965, 0.9247)$
	3	$22.513\%, (0.6289, 0.7174, -0.2997)$	$19.817\%, (0.6601, 0.7147, -0.2310)$
AWS13	1	$46.536\%, (0.6499, -0.7084, -0.2753)$	$49.149\%, (0.6670, -0.7072, -0.2344)$
	2	$33.433\%, (0.3966, 7.106 \cdot 10^{-3}, 0.9179)$	$33.323\%, (0.3323, 8.263 \cdot 10^{-4}, 0.9432)$
	3	$20.030\%, (0.6483, 0.7058, -0.2856)$	$17.507\%, (0.6668, 0.7070, -0.2356)$
Amundsen-Scott	1	$41.559\%, (0.5312, -0.6865, -0.4965)$	$44.738\%, (0.6186, -0.6952, -0.3660)$
	2	$32.442\%, (0.6760, 9.893 \cdot 10^{-3}, 0.7368)$	$32.631\%, (0.4735, -0.04183, 0.8798)$
	3	$25.999\%, (0.5108, 0.7270, -0.4588)$	$22.631\%, (0.6270, 0.7176, -0.3033)$
Vostok	1	$43.258\%, (0.6251, -0.7272, -0.2836)$	$47.037\%, (0.6660, -0.7172, -0.2052)$
	2	$34.717\%, (0.4871, 0.07950, 0.8697)$	$34.321\%, (0.3657, 0.07418, 0.9278)$
	3	$22.025\%, (0.6099, 0.6818, -0.4039)$	$18.642\%, (0.6502, 0.6929, -0.3117)$

Table 13: The first, second, and third EOFs for wind speed, SAM, and SOI at each station, with the percent of the variance represented by each EOF given with each vector.

Station	EOF	Wind speed
AWS8	1	$42.749\%, (0.5675, -0.6741, -0.4728)$
	2	$31.789\%, (0.6035, -0.05012, 0.7958)$
	3	$25.463\%, (0.5601, 0.7369, -0.3784)$
AWS9	1	$44.903\%, (0.6099, -0.6728, -0.4189)$
	2	$31.500\%, (0.4787, -0.1084, 0.8712)$
	3	$23.597\%, (0.6315, 0.7319, -0.2560)$
AWS12	1	$43.514\%, (0.6253, -0.7238, -0.2917)$
	2	$34.471\%, (0.4836, 0.06600, 0.8728)$
	3	$22.015\%, (0.6125, 0.6868, -0.3913)$
AWS13	1	$42.195\%, (0.6050, -0.7344, -0.3076)$
	2	$35.038\%, (0.5307, 0.08392, 0.8434)$
	3	$22.767\%, (0.5936, 0.6735, -0.4405)$
Amundsen-Scott	1	$41.671\%, (0.5431, -0.6990, -0.4653)$
	2	$32.962\%, (0.6448, -7.776 \cdot 10^{-3}, 0.7643)$
	3	$25.367\%, (0.5379, 0.7151, -0.4465)$
Vostok	1	$39.084\%, (0.2812, -0.6838, -0.6733)$
	2	$32.857\%, (0.9579, 0.1576, 0.2400)$
	3	$28.059\%, (0.05798, 0.7124, -0.6993)$

7 Summary and conclusions

This study has used time series data from six weather stations on the Plateau – IMAU AWS 8, 9, 12, and 13, and Amundsen-Scott and Vostok Stations – together with ERA5 reanalysis products to investigate the variability and trends of the East Antarctic Plateau climate, and how the SAM and SO impact the climate of the Plateau. The focus was primarily on near-surface (potential) temperature, near-surface wind speed, and snow accumulation, with a secondary focus on surface air pressure.

Observational and ERA5 time series at each station site were compared using calculations of bias, $RMSD$, and linear least-squares regressions. Despite some flaws in the comparability of these datasets, strong agreements were found for temperature, surface pressure, and the SOI. Likely due to the difference in their derivations, the observational and ERA5-derived SAM indices had a weaker – but reasonable – degree of agreement. Comparisons for wind speeds were inconsistent, likely due to a combination of sensor heights not matching the ERA5 10m wind speed height, topographic height differing between the stations and their respective ERA5 grid boxes, and local surface features and slopes not being well-replicated by ERA5.

Even for the shorter AWS records, the (approximate) monthly climtological averages for obesrved near-surface (potential) temperatures produced the expected patterns, with long "coreless" winters, short summers, and rapid transitions between. Lower (potential) temperatures and larger differences between summer and winter were generally found for higher elevation and farther inland sites, with the unique topography surrounding Vostok Station resulting in the lowest (potential) temperatures. While average summer potential temperatures were very similar at all sites, the lower winter values at the upper Plateau stations illustrate the larger radiative cooling and stronger temperature inversion present on the upper Plateau. The shorter AWS records appear to be more of a limitation for wind speeds and monthly net snow accumulation. The observational (approximate) wind speed climatologies broadly follow the expected pattern of higher speeds during colder months and lower speeds during warmer months, with some inconsistent indication of lower wind speeds higher on the Plateau. The (approximate) climatologies for monthly net snow accumulation do not show any clear pattern with respect to elevation or distance inland, and do not closely agree with regard to a yearly cycle. In general, large amounts of accumulation occur during the transition from summer to winter as the falling temperatures reduce the moisture capacity of the air, with additional peaks in mid-winter, and another period of increased snowfall during the transition from winter to summer as advection of moisture to the region increases. Low amounts of accumulation or months with net removal occur between the periods of high accumulation, with very little moisture available following precipitation events.

The time series for observed (potential) temperature showed very strong seasonal cycles that closely followed the (approximate) climatology at each station, and had no significant linear trends with respect to time, possibly because of the seasonal cycle dominating possible signals. The wind speed time series had significant trends at only three stations, all of which were downward trends with weak correlations. Time series for monthly net snow accumulation showed no clear yearly cycles and no significant trends with respect to time.

For observational data and the SAM, significant correlations were found for (potential) temperature at all sites except AWS8, for wind speed only at AWS9 and Amundsen-Scott Station, and for net snow accumulation only at AWS9, suggesting that the SAM has a detectable effect on (potential) temperatures on the Plateau, but more limited influence on wind speed and snow

accumulation. The correlations for (potential) temperature were consistently stronger for stations farther inland, and were also stronger for temperature than for potential temperature. The two correlations between wind speed and the SAM were both negative, which was consistent with expectations, but both are also weak, and provide little information on possible spatial patterns. The one correlation found for monthly net snow accumulation and the SAM was weak and positive, despite the expectation that less precipitation would occur during the positive SAM phase. No significant correlations were found between the observational data and the SOI, suggesting a limited influence of the SO on the Plateau.

The EOF analyses for the observational data agreed with and reinforced the findings based on linear regressions with the indices. The influence of the indices was primarily evident for (potential) temperature, with the SAM being found to be dominant farther inland, and the SO being closer to equal – but still secondary – in the lower parts of the Plateau. Increasing SAM was strongly associated with decreasing (potential) temperature, and decreasing SAM with increasing (potential) temperature. The (often much) weaker associations with the SOI showed mixed influence, with negative associations in the first and third EOFs and positive associations in the second EOFs. Not all expected results were found (i.e. for wind speed and snow accumulation), but the findings for (potential) temperatures are consistent with expectations.

The monthly climatological averages for ERA5 2m (potential) temperature gave results very similar to those for observed near-surface (potential) temperature, but with slightly warmer winters and slightly colder summers. ERA5 10m wind speed climatologies show much clearer seasonal cycles than the observational wind speed, with higher wind speeds in winter and lower speeds in summer, as well as a clearer pattern of lower wind speeds in the relatively flat upper regions of the Plateau and higher winds speeds in the katabatic zone lower on the Plateau. The climtologies for ERA5 snowfall also showed much clearer results than those for observed net snow accumulation. The largest amounts of snowfall occur as temperatures fall during the transition to winter, followed by small amounts during the winter itself, an increase in snowfall during the transition to summer as moisture advection to the region is increasing, and finally reduced snowfall during the summer. The sites lower on the Plateau (AWS 8 and 9, and Amundsen-Scott Station) had snowfall climatologies with maxima approximately to to three times larger than the maxima for sites on the upper Plateau (AWS 12 and 13, and Vostok Station), due to the more extreme cold and dry conditions on the upper Plateau. Snowfall correlations between stations, however, are few and weak. The ERA5 snowfall climatologies have maxima nearly two orders of magnitude smaller than the maxima for observed net snow accumulation; the reasons for this are unclear.

Similar to observed (potential) temperature, the time series for ERA5 2m (potential) temperature display strong seasonal cycles and had no significant trends with respect to time. The ERA5 10m wind speed time series had significant trends with respect to time at all locations except AWS8; contrary to the findings for observed wind speeds, all of these are weak positive trends, suggesting that near-surface wind speeds at different heights could have different temporal trends. Time series for ERA5 monthly total snowfall display yearly cycles corresponding to their climatologies, though not as strongly as (potential) temperature; no significant temporal trends were found for snowfall at any site.

Significant correlations between the SAM and ERA5 data were found for 2m (potential) temperature at all sites, 10m wind speed at all except Vostok Station, and snowfall only and AWS 8 and 13, suggesting that the SAM has a detectable effect on (potential) temperatures and wind speeds over much of the Plateau, but a more limited influence on snowfall. The correlations for

2m (potential) temperature are stronger farther inland, and are stronger for temperature than for potential temperature. The observed (potential) temperatures generally had stronger correlations with the SAM than did the ERA5 2m (potential) temperatures. 10m wind speeds were found to be negatively correlated with the SAM, but had no clear connection between correlation strength and either elevation or distance inland. The correlations for snowfall were weak, with one positive and one negative despite the expectation that snowfall would be negatively correlated with the SAM. The only correlations found for ERA5 data with the SOI were two for snowfall, both weak and positive, which did agree with expectations.

EOF analyses for the ERA5 data again agreed with and reinforced the results of the linear regressions with the indices. When influence from the indices was detected, the SAM was found to be more dominant farther inland, with the effect of the SO closer to equal lower on the Plateau. Both the SAM and SO appeared to have limited influence on Plateau snowfall. However, strong associations were found for 2m (potential) temperature and 10m wind speed with the SAM, with these variables found to decrease with increasing SAM and increase with decreasing SAM. All were found to have the same mixed associations with the SOI, as was found for the observational (potential) temperature. With the exception of the lack of findings for snowfall, all of these results were consistent with expectations. These findings also agree well with the observational results for (potential) temperature.

8 Opportunities for further investigation

Over the course of conducting this study, several possibilities for further investigation have been identified, which were not explored in this study due to limitations of scope. These possibilities are briefly described here.

1. **Additional stations:** As mentioned in section 2.1, meteorological records are available for a small number of Plateau stations that were not used in this study. Including these additional Plateau stations could have led to a more complete examination of the Plateau climate and how it is influenced by the SAM and SO. Furthermore, the focus of this study has been on the East Antarctic Plateau in particular, but it would also be of value to expand the scope to include stations on the Antarctic Peninsula, West Antarctica, and coastal East Antarctica, since doing so would allow for broader insights into the climate of the Antarctic continent as a whole.

2. **Alternative ERA5 SAM index definition:** For the sake of comparison with the observational SAM index (definition shown in section 2.2.2), it would be beneficial to use ERA5 data from the same locations to produce approximate zonal means for sea-level pressure using the same calculations as the observational SAM index, rather than using all zonal grid points at exact latitude coordinates. The latter method was used in this study, to more closely approximate a theoretical ideal SAM index calculation, but made it difficult to determine how well ERA5 is able to reproduce the observational SAM index.

3. **Sensitivity of ERA5 SOI to coordinates:** It is possible that the ERA5-derived SOI would prove to be sensitive to the ERA5 coordinates chosen to represent the Darwin and Tahiti measurement sites. Assessing this possibility could lead to improved understanding of why a stronger agreement was not found between the observational and ERA5-derived SO indices. (A similar investigation of sensitivity to ERA5 coordinates would also be valuable for the alternative calculation of the ERA5 SAM index suggested in point 2.)

4. **Including surface air pressure:** With the exceptions of AWS 12 and 13, all stations used in this study also provide time series for surface air pressure. These data are used for comparison with ERA5 surface pressure at these locations in section 4.2 and were used to calculate potential temperatures, but surface pressure data were not utilized further. Applying the methods used in sections 5 and 6 to observational and ERA5 surface pressure time series would provide a more complete understanding of the local meteorological conditions at these sites and the impacts of the SAM and SO on the region.

5. **Surface slope data:** Because the surface slope is one of the main drivers of climate in Antarctica, more precise data about the local surface slope at each station (if available) would allow for improved analysis of all results found in this study.

6. **SAM and SOI temporal trends:** Sections 5.2 and 6.2 investigated possible temporal trends in the primary meteorological variables of focus (from observations and ERA5, respectively), but not for the observational and ERA5-derived SAM and SO indices. Investigating the ERA5-derived SAM index would be of particular interest, in order to determine whether it shows an upward trend similar to that which has been found in the observational SAM index (e.g. Fogt and Marshall, 2020; Marshall, 2003)[9][17].

7. **Deseasonalized time series, and temporal trend detection:** Because seasonal cycles – particularly for (potential) temperature – increase the difficulty of detecting possible temporal trends, subtracting the seasonal component before performing linear regression on a time series could improve detection of these trends.

8. **Annual and seasonal trends:** Examining annual mean time series could enable detection of trends that could not be found by looking only at monthly mean time series. Similarly, investigating possible trends in each austral season (Dec.-Feb., Mar.-May, June-Aug., Sep.-Nov.) could show changes that cannot be detected in monthly data, but which are still limited to certain times of year. Both of these approaches are common is investigations of the SAM and SO impacts on Antarctica (e.g. Fogt and Marshall, 2020; Jones et al., 2019; Schneider et al., 2012b; van den Broeke and van Lipzig, 2004; Welhouse et al., 2016)[9][14][29][36][38].

9. **Expanding spatial coverage with ERA5:** Though the ERA5 reanalysis offers data with spatial coverage far superior to what Antarctic stations can provide, this study made use of ERA5 products only at the approximate locations of the stations used. However, taking advantage of this spatial coverage would enable investigations of the effects of the SAM and SO to include every ERA5 grid point in the entire Antarctic region. Part of the investigation by Jones et al. (2019) was similar to this, using HadISST1 data for sea surface temperature and ERA-Interim reanalysis data for monthly mean sea-level pressure and 500-hPa geopotential height to explore linear trends across the Southern Ocean, along with weather station data from Antarctica and the southern midlatitudes. Using ERA5 data to expand this study could lead to results that better illustrate spatial patterns and local effects for (potential) temperature, surface pressure, wind speed, and snowfall.

References

[1] Arctic and Antarctic Research Institute. http://aari.aq/stations/vostok/vostok_en.html. Retrieved March 20, 2021.

[2] Bolton, D. 1980. "The computation of equivalent potential temperature". *Monthly Weather Review*, **108**, 1046–1053.

[3] Bromwich, D.H., and Fogt, R.L. 2004. "Strong trends in the skill of the ERA-40 and NCEP–NCAR reanalyses in the high and midlatitudes of the Southern Hemisphere, 1958–2001". *J. Climate*, **17**, 4603–4619, https://doi.org/10.1175/3241.1.

[4] Bromwich, D.H., Nicolas, J.P., Monaghan, A.J., Lazzara, M.A., Keller, L.M., Weidner, G.A., and Wilson, A.B. 2013. "Central West Antarctica among the most rapidly warming regions on Earth". *Nat. Geosci.*, **6**, 139–145, https://doi.org/10.1038/ngeo1671.

[5] Bromwich, D.H., Nicolas, J.P., Monaghan, A.J., Lazzara, M.A., Keller, L.M., Weidner, G.A., and Wilson, A.B. 2014. "Corrigendum: Central West Antarctica among the most rapidly warming regions on Earth". *Nat. Geosci.*, **7**, 76, https://doi.org/10.1038/ngeo2016.

[6] Carrasco, J.F. 2013. "Decadal changes in the near-surface air temperature in the western side of the Antarctic Peninsula". *Atmos. Climate Sci.*, **3**, 275–281, https://doi.org/10.4236/acs.2013.33029.

[7] Ding, M., Yang, D., van den Broeke, M.R., Allison, I., Xiao, C., Qin, D., and Huai, B. 2020. "The surface energy balance at Panda 1 Station, Princess Elizabeth Land: A typical katabatic wind region in East Antarctica". *Journal of Geophysical Research: Atmospheres*, **125**, e2019JD030378. https://doi.org/ 10.1029/2019JD030378

[8] Fogt, R.L., Bromwich, D.H., and Hines, K.M. 2011. "Understanding the SAM influence on the South Pacific ENSO teleconnection". *Climate Dyn.*, **36**, 1555–1576, https://doi.org/10.1007/s00382-010-0905-0.

[9] Fogt, R.L., and Marshall, G.J. 2020. "The Southern Annular Mode: Variability, Trends, and Climate Impacts Across the Southern Hemisphere". *Wiley Interdisciplinary Reviews: Climate Change*, **11** (4). doi:10.1002/wcc.652.

[10] Hersbach, H., Bell, B., Berrisford, P., Biavati, G., Horányi, A., Muñoz Sabater, J., Nicolas, J., Peubey, C., Radu, R., Rozum, I., Schepers, D., Simmons, A., Soci, C., Dee, D., Thépaut, J-N. (2019): ERA5 monthly averaged data on single levels from 1979 to present. Copernicus Climate Change Service (C3S) Climate Data Store (CDS). (Accessed on 02-04-2021), 10.24381/cds.f17050d7

[11] Holland, M.M., and Bitz, C.M. 2003. "Polar amplification of climate change in coupled models". *Climate Dyn.*, **21**, 221–232, https://doi.org/10.1007/s00382-003-0332-6.

[12] Institute for Marine and Atmospheric Research Utrecht, Ice and Climate group, Utrecht University. n.d. "Antarctic stations". Accessed March 20, 2021. http://www.projects.science.uu.nl/iceclimate/aws/antarctica.php.

[13] Institute for Marine and Atmospheric Research Utrecht, Ice and Climate group, Utrecht University. n.d. "Technical information". Accessed June 29, 2021. http://www.projects.science.uu.nl/iceclimate/aws/technical.php.

[14] Jones, M.E., Bromwich, D.H., Nicolas, J.P., Zou, X., Wang, S.-H., Carrasco, J., and Plavcova, E. 2019. "Sixty Years of Widespread Warming in the Southern Middle and High Latitudes (1957-2016)". *Journal of Climate*, **32** (20). doi:10.1175/JCLI-D-18-0565.1.

[15] Kwok, R., and Comiso, J.C. 2002. "Spatial Patterns of Variability in Antarctic Surface Temperature: Connections to the Southern Hemisphere Annular Mode and the Southern Oscillation". *Geophysical Research Letters*, **29** (14): 50–51. doi:10.1029/2002GL015415.

[16] Lazzara, M. A., Keller, L. M., Markle, T., and Gallagher, J. 2012. "Fifty-year Amundsen–Scott South Pole station surface climatology". *Atmos. Res.*, **118**, 240–259, https://doi.org/10.1016/j.atmosres.2012.06.027.

[17] Marshall, G.J. 2003. "Trends in the Southern Annular Mode from Observations and Reanalyses". *J. of Climate*, **16**, 4134-4143.

[18] Marshall, G.J. 2007. "Half-century seasonal relationships between the southern annular mode and Antarctic temperatures". *Int. J. Climatol.*, **27**, 373–383, https://doi.org/10.1002/joc.1407.

[19] Marshall, G.J., Orr, A., and Turner, J. 2013. "A predominant reversal in the relationship between the SAM and East Antarctic temperatures during the twenty-first century". *J. Climate*, **26**, 5196–5204, https://doi.org/10.1175/JCLI-D-12-00671.1.

[20] Marshall, G.J., and Bracegirdle, T.J. 2015. "An Examination of the Relationship between the Southern Annular Mode and Antarctic Surface Air Temperatures in the Cmip5 Historical Runs". *Climate Dynamics : Observational, Theoretical and Computational Research on the Climate System*, **45** (5-6): 1513–35. https://doi.org/10.1007/s00382-014-2406-z.

[21] Marshall, G.J., and Thompson, D.W.J. 2016. "The signatures of large-scale patterns of atmospheric variability in Antarctic surface temperatures". *J. Geophys. Res. Atmos.*, **121**, 3276-3289, doi:10.1002/2015JD024665.

[22] Marshall, G.J. n.d. "An observation-based Southern Hemisphere Annular Mode Index". https://legacy.bas.ac.uk/met/gjma/sam.html. Retrieved January 11, 2021.

[23] Medley, B, and E. R Thomas. 2019. "Increased Snowfall Over the Antarctic Ice Sheet Mitigated Twentieth-Century Sea-Level Rise". *Nature Climate Change*, **9** (1): 34–39. doi:10.1038/s41558-018-0356-x.

[24] Muñoz Sabater, J., (2019): ERA5-Land monthly averaged data from 1981 to present. Copernicus Climate Change Service (C3S) Climate Data Store (CDS). (Accessed 08-06-2021), 10.24381/cds.68d2bb3

[25] National Centers for Environmental Information, National Oceanic and Atmospheric Administration. n.d. https://www.ncdc.noaa.gov/teleconnections/enso/indicators/soi/. Retrieved January 11, 2021.

[26] National Science Foundation. n.d. https://www.nsf.gov/geo/opp/support/southp.jsp. Retrieved March 20, 2021.

[27] Norwegian-U.S. Scientific Traverse of East Antarctica, via Internet Archive. n.d. https://web.archive.org/web/20131005002746/http://traverse.npolar.no/. Retrieved April 03, 2021.

[28] Schneider, D.P., Deser, C., and Okumura, Y. 2012a. "An assessment and interpretation of the observed warming of West Antarctica in the austral spring". *Climate Dyn.*, **38**, 323–347, https://doi.org/10.1007/s00382-010-0985-x.

[29] Schneider, D.P., Okumura, Y., and Deser, C. 2012b. "Observed Antarctic Interannual Climate Variability and Tropical Linkages". *Journal of Climate*, **25** (12): 4048–66.

[30] SciPy Community, The. 2021. "scipy.stats.linregress". Documentation. Updated April 26, 2021. https://docs.scipy.org/doc/scipy/reference/generated/scipy.stats.linregress.html

[31] Serreze, M. C., Barrett, A. P., Stroeve, J. C., Kindig, D.N., and Holland, M. M. 2009. "The emergence of surface-based Arctic amplification". *Cryosphere*, **3**, 11–19, https://doi.org/10.5194/tc-3-11-2009.

[32] Smith, K.L., and Polvani, L.M. 2017. "Spatial patterns of recent Antarctic surface temperature trends and the importance of natural variability: Lessons from multiple reconstructions and the CMIP5 models". *Climate Dyn.*, **48**, 2653–2670, https://doi.org/10.1007/s00382-016-3230-4.

[33] Turner, J., and Coauthors, 2004: The SCAR READER Project: Toward a high-quality database of mean Antarctic meteorological observations. *J. Climate*, **17**, 2890–2898, https://doi.org/10.1175/1520-0442(2004)017<2890:TSRPTA>2.0.CO;2.

[34] Turner, J., Anderson, P., Lachlan-Cope, T., Colwell, S., Phillips, T., Kirchgaessner, A., Marshall, G.J., King, J.C., Bracegirdle, T., Vaughan, D.G., Lagun, V., and Orr, A. 2009. "Record low surface air temperature at Vostok station, Antarctica". *J. Geophys. Res.*, **114**, D24102, doi:10.1029/2009JD012104.

[35] van den Broeke, M.R. 2000. "The semi-annual oscillation and the Antarctic Climate. Part 3: The role of near-surface wind speed and cloudiness". *Int. J. Climatol.*, **20**: 117-130.

[36] van den Broeke, M.R., and van Lipzig N.P.M. 2004. "Changes in Antarctic Temperature, Wind and Precipitation in Response to the Antarctic Oscillation". *Annals of Glaciology*, **39**: 119–26. doi:10.3189/172756404781814654.

[37] van den Broeke, M., Reijmer, C., van As, D., and Boot, W. 2006. "Daily Cycle of the Surface Energy Balance in Antarctica and the Influence of Clouds". *Int. J. Climatol.*, **26**: 1587-1605. doi:10.1002/joc.1323

[38] Welhouse, L.J., Lazzara, M.A., Keller, L.M., Tripoli, G.J., and Hitchman, M.H. 2016. "Composite Analysis of the Effects of ENSO Events on Antarctica". *Journal of Climate*, **29** (5): 1797–1808.

[39] Yuan, X., Kaplan, M.R., and Cane, M.A.. 2018. "The Interconnected Global Climate System—a Review of Tropical-Polar Teleconnections". *Journal of Climate*, **31** (15): 5765–92.